Acoustic Indoor Localization Based on Range and Relative Velocity in Non-Line-of-Sight Environment

Lei Zhang, Hucheng Wang, *Member, IEEE*, Wei He, and Xinheng Wang, *Senior Member, IEEE*

***Abstract*—This article investigates the problem of acoustic indoor localization in dense non-line-of-sight (NLOS) environments by using range and relative velocity measurements obtained from received acoustic signals, without the need for additional sensors. The relationship between adjacent positions to be estimated is established by introducing velocity measurements and assuming a first-order motion model. This reduces the number of required line-of-sight (LOS) anchors. The principle of the range and relative velocity-based localization method is systematically studied and a basic solution based on a least square estimator (LSE) and its closed-form has been proposed. In order to achieve precise localization in dense NLOS environments, a multiposition joint estimation (MPJE) method is proposed. This method involves jointly estimating multiple positions in a short-time position sequence and is solved using a Levenberg–Marquardt (LM) algorithm. A LOS measurements redundancy metric is proposed to balance the localization accuracy and algorithm time cost by adjusting the sequence length. The results obtained from numerical simulations and experimental investigations demonstrate that the proposed range and relative velocity-based localization method outperforms the conventional range-based methods. The number of required LOS anchors for accurate localization is reduced from 3 to 2 for 2-D positioning. In addition, the proposed MPJE method requires only two LOS anchors and permits the use of only one LOS anchor for a short period. This enables its application in dense NLOS environments with a low anchor deployment density, thereby increasing its scene adaptive capability and promotional value.**

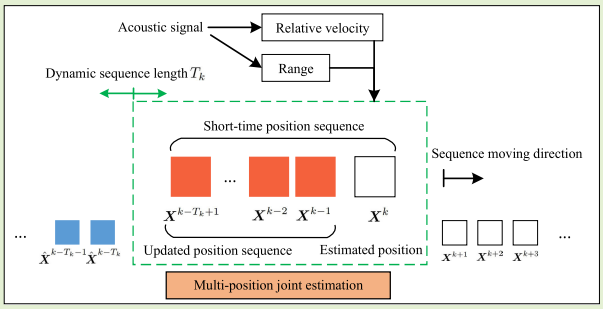

***Index Terms*— Acoustic, indoor localization, non-line-of-sight (NLOS), range, relative velocity.**

I. Introduction

WIDE applications of smart devices, such as smartphones, smartwatches, floor-mopping robots, and other smart devices, have recently received much attention. Accurate indoor localization has become a significant area of research. Various approaches have been proposed based on the inertial measurement unit (IMU) [1], ultra-wide-band (UWB) [2], Bluetooth, pedestrian dead reckoning (PDR) [3], WiFi, global system for mobile (GSM) communications, acoustic [4], [5], [6], light, and magnetic fields [7]. Among these approaches, acoustic localization technology has attracted researchers' attention due to its advantages of being fully compatible with commercial off-the-shelf (COTS) smart devices, having relatively higher positioning accuracy, and lower cost infrastructure [8]. Numerous prototype systems have been developed to advance the development and application of acoustic indoor localization technology in real-world scenarios.

The methods of acoustic indoor localization systems mainly include time of arrival (TOA), time difference of arrival (TDOA), and direction of arrival (DOA). The range (TOA)-based positioning method is very popular and typically provides satisfactory performance with accuracy at the decimeter level in real-world scenarios [9]. Among those acoustic indoor localization systems, most of them use TOA of an

Manuscript received 21 March 2024; revised 21 April 2024; accepted 23 April 2024. Date of publication 3 May 2024; date of current version 14 June 2024. This work was supported in part by the National Natural Science Foundation of China (NSFC) under Grant 62003053 and Grant 52175030, in part by the Shaanxi Provincial Natural Science Basic Research Program under Grant 2020JQ-389, and in part by the Chinese Academy of Sciences (CAS) Key Laboratory Project Fund under Grant 20200604. The associate editor coordinating the review of this article and approving it for publication was Prof. Yulong Huang. *(Corresponding author: Lei Zhang.)*

Lei Zhang is with the School of Construction Machinery, Chang'an University, Xi'an 710064, China (e-mail: zhlei0202@163.com).

Hucheng Wang is with the College of Control Science and Engineering, Zhejiang University, Hangzhou 310027, China (e-mail: hcwang@bit.edu.cn).

Wei He is with the Shanghai Institute of Microsystem and Information Technology, Chinese Academy of Sciences, Shanghai 201899, China (e-mail: wei.he@mail.sim.ac.cn).

Xinheng Wang is with the School of Advanced Technology, Xi'an Jiaotong-Liverpool University, Suzhou 215000, China (e-mail: xinheng.wang@xjtlu.edu.cn).

Digital Object Identifier 10.1109/JSEN.2024.3393992

© 2024 The Authors. This work is licensed under a Creative Commons Attribution-NonCommercial-NoDerivatives 4.0 License.
For more information, see https://creativecommons.org/licenses/by-nc-nd/4.0/

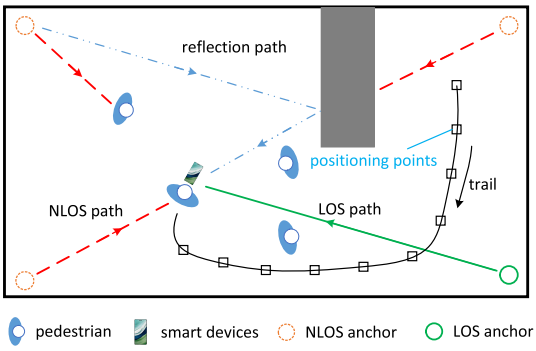

Fig. 1. Simplified diagram of the real indoor localization scenario.

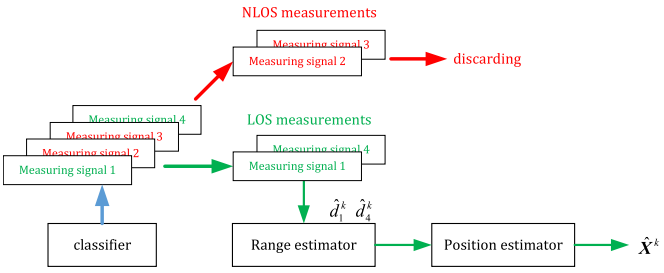

Fig. 2. Basic NLOS localization procedure with identifying-discarding approach.

acoustic chirp signal to realize ranging-based positioning [10], [11], [12], [13].

It is evident that non-line-of-sight (NLOS) will introduce considerable positioning errors. Fig. 1 depicts a pedestrian carrying a smart device walking around in an indoor environment. In fact, it is common that the line-of-sight (LOS) path, or direct path, is obstructed by human bodies, furniture, walls, or corners, due to the arbitrariness of human movement. NLOS phenomenon poses a serious challenge to the practical applications of acoustic indoor localization systems, which can also be demonstrated by the results of the Microsoft Indoor Localization Competition [14].

The NLOS localization problem has been extensively discussed in the area of wireless indoor localization, and many methods have been proposed [15] to address this issue. Filtering algorithms are commonly employed to mitigate NLOS effects, which constitute a significant category of methods. The robust Kalman filtering framework based on student's t distribution [16], Gaussian-student's t mixture distribution [17], and statistical similarity measure [18] is specifically designed to handle nonstationary heavy-tailed measurement noise resulting from NLOS and stand out as the most promising approaches for addressing the NLOS mitigation challenge.

The simplest way of NLOS localization is achieved by identifying and discarding the NLOS measurements, and estimating the position of the target by using one of the LOS localization techniques, such as the maximum likelihood algorithm and least squares techniques [19]. The basic procedure is illustrated in Fig. 2.

By identifying and discarding the NLOS measurements, the range-based indoor localization system can greatly improve its performance and stability by utilizing only LOS measurements. NLOS identification methods based on support vector machine (SVM), label propagation algorithm based SVM (LPA-SVM), and Gaussian mixture model (GMM) can achieve satisfactory accuracy in real-world acoustic channel conditions [8], [20]. Discarding NLOS measurements means only a few LOS measurements are used for the positioning algorithm, which poses a challenge for many positioning methods because at least three measurements are required for the calculation.

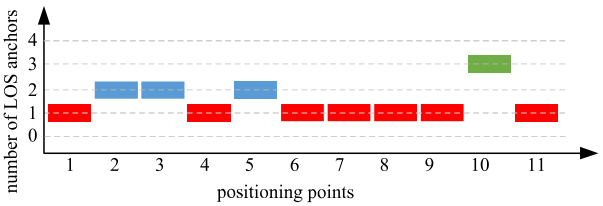

Fig. 3. Number of LOS anchors available at each positioning point.

For the simplified scenario shown in Fig. 1, we assume that when the pedestrian carrying a smart device walks along the trail, other pedestrians stand still. The number of LOS anchors that can be used for the positioning algorithm at each positioning point is shown in Fig. 3. Even though there are four anchors deployed in the scene, only one LOS anchor can be used due to the uncertainties of pedestrians in most cases. In this condition, the NLOS localization problem can be considered as a localization problem under a low density of LOS anchor nodes. How to realize accurate indoor localization in such insufficient LOS anchors is the most critical challenge that needs to be addressed in practical applications.

In order to achieve accurate positioning for low-cost commercial devices under the condition of insufficient LOS anchors, it is essential to introduce additional sources of data to increase the information required for target localization without adding additional sensors. Fortunately, the slower speed of sound propagation allows the motion of the smart devices to be easily represented by the Doppler shift in the received acoustic signals. This enables simultaneous measurements of the range and relative velocity between smart devices and anchors. The relative velocity, referred to as the frequency of arrival (FOA), is obtained by estimating the Doppler shift of acoustic signals.

In the field of localization, there is still a lack of unified terminologies for measurements. The range measurement can also be referred to as time delay and TOA measurement. The measurement of relative velocity can also be referred to as either Doppler-shift measurement or FOA. For the sake of consistency, this article collectively refers to these two types of measurements as range and relative velocity measurements.

In earlier studies, research of target localization using range and relative velocity measurements is mainly centered on the Galileo search and rescue system [21], [22], [23]. Utilization and investigation of active target detection and tracking, which employ range and relative velocity, have been widely conducted in radar research [24], [25]. Range and relative velocity are also introduced to estimate the position and velocity of moving targets based on sensors in motion

[26], [27]. A direct position determination approach to efficiently realize the target position estimation based on range and relative velocity measurements was presented in [28]. Based on a single moving station, a structural total least square algorithm for locating multiple disjoint sources was presented by using AOA, range, and relative velocity measurements [29]. Although the application scenarios of these methods differ from indoor localization, they provide insights and guidance for studying indoor localization techniques based on range and relative velocity.

For passive target localization, an importance sampling method based on range and relative velocity measurements was presented in [30]. A Lagrange programming neural network framework to address the problem of estimating the position and velocity of a moving source using range and relative velocity measurements was presented [31]. By exploiting both range and relative velocity measurements, a weighted least square method was formulated to jointly estimate the source position, velocity, clock bias, and clock drift, which was efficiently solved using semi-definite relaxation [32]. While these methods perform well in LOS scenarios, their effectiveness is significantly compromised in NLOS environments or low-density deployment of anchors.

For the NLOS localization scenario, a least square algorithm to estimate the target location using measurements of range, DOA, and relative velocity was presented in [33]. This method could achieve rough localization of mobile phones by using NLOS communication signals, without directly tackling the NLOS localization problem. In [34], a particle filtering (PF) method was proposed by using range and relative velocity for acoustic indoor localization in the NLOS environment. However, the method is significantly impaired by measurement noise and fails to produce satisfactory results in large-scale scenarios.

In contrast to those previous work, this article focuses on how to achieve accurate and stable localization in dense NLOS environments, while utilizing significantly fewer LOS anchors. A novel indoor localization approach based on range and relative velocity measurements without the need for additional sensors was proposed. The main advantage of the proposed method is that it achieves 2-D positioning using only two LOS anchors, and allows only one LOS anchor for a short period of time. This enables its application in dense NLOS environments with a low anchor deployment density, thereby increasing its scene adaptive capability and promotional value. By using this method, the problem illustrated in Fig. 1 could be well addressed.

The main contributions of this research are summarized as follows.

1) A novel acoustic indoor localization approach based on range and relative velocity measurements is proposed and studied systematically, without the need for additional sensors. The basic least square solution and its closed-form solution are derived, respectively. Compared to conventional range-based localization methods, the proposed method reduces the number of required LOS anchors for accurate localization from 3 to 2 for 2-D positioning.
2) To achieve precise localization in dense NLOS environments, a multiposition joint estimation (MPJE) method is proposed by jointly estimating the multiple positions in a short-time position sequence, and solved by using the Levenberg–Marquardt (LM) algorithm. The proposed method could break the error propagation and accumulation chain, require only two LOS anchors, and permit the use of only one LOS anchor for a short period.
3) An LOS measurement redundancy metric is proposed to balance the localization accuracy and algorithm time cost through the adjustment of the sequence length.

Results from numerical simulations and experiments show that the proposed acoustic indoor localization methods are not only suitable for dense NLOS localization scenarios but also capable of achieving accurate localization under low anchor deployment density conditions.

The remainder of the article is organized as follows. In Section II, we first introduce how to simultaneously estimate the range and relative velocity measurements from the received acoustic signals. To realize localization based on range and relative velocity measurements, we have provided a maximum likelihood solution, a least square solution, and a closed-form solution. Section III introduces the MPJE method and explains the calculation process in detail. Sections IV and V present the numerical simulations and experiments to evaluate the performance of our proposed methods. Finally, we summarize our conclusion in Section VI.

II. Range and Relative Velocity-Based NLOS Localization

A. Acoustic NLOS Localization From Identifying and Discarding Perspective

For an acoustic indoor localization system, assuming N range measurements obtained from anchors predeployed in the environment can be used to estimate the target's position $\boldsymbol{X}^k$ at kth time. In addition, the number of range measurements obtained from NLOS anchors is M, where $0 \leq M \leq N$. By identifying and discarding the NLOS range measurements, we can use the remaining $N - M$ LOS range measurements to estimate $\boldsymbol{X}^k$. The NLOS localization problem with N predeployed anchors can be considered as an LOS localization problem with $N-M$ anchors. Clearly, this presents an acoustic localization problem with a low density of anchor deployment.

Typically, $N = 4$ or $N = 3$ should be guaranteed in a practical 2-D localization application, which is obtained by taking into consideration the tradeoff between system deployment cost, localization update frequency, and user experience. However, in dense NLOS environments, obtaining sufficient three LOS range measurements to ensure the performance of positioning algorithms becomes challenging, because of the complexity and dynamic nature of indoor environments.

Therefore, addressing the acoustic NLOS localization challenge in real applications requires the realization of acoustic indoor localization with a low density of anchor deployment, specifically less than three LOS anchors. We aim to solve this problem without the need for additional sensors by using range

and relative velocity measurements obtained from acoustic signals.

B. Range and Relative Velocity Measurements Estimation

While most acoustic indoor localization systems utilize linear frequency modulation (LFM) signals for ranging, hyperbolic frequency modulation (HFM) signals are preferable for range and velocity measurement. HFM signals offer the Doppler-invariant property, enabling simultaneous ranging and relative velocity measurement [35].

The complex form of an HFM signal can be written as

$$r(t) = \begin{cases} \exp\left\{-j2\pi K \ln\left(1-\frac{t}{G}\right)\right\}, & -\frac{T}{2} \le t \le \frac{T}{2} \\ 0, & \text{otherwise} \end{cases} \quad (1)$$

where

$$G = \frac{T(f_h + f_l)}{2(f_h - f_l)}, \quad K = \frac{T f_l f_h}{f_h - f_l} \quad (2)$$

f_l and f_h are the lowest and the highest frequency of the HFM signal, respectively. T is the time duration.

In order to realize simultaneous ranging and relative velocity measurement, the transmitted signal $s(t)$ should include two different HFM components, which is given by

$$s(t) = \cos\left(-2\pi K_1 \ln\left(1-\frac{t-T/2}{G_1}\right)\right) + \cos\left(-2\pi K_2 \ln\left(1-\frac{t-T/2}{G_2}\right)\right) \quad (3)$$

where $0 \le t \le T$, and the two HFM components are denoted as HFM_1 and HFM_2, respectively.

Assuming the time delay of $s(t)$ is τ_i^k, the time delay estimation of HFM_1 and HFM_2 are $\hat{\tau}_{i,1}^k$ and $\hat{\tau}_{i,2}^k$, respectively, which are given by

$$\begin{cases} \hat{\tau}_{i,1}^k = \tau_i^k - \frac{\alpha_i^k}{1+\alpha_i^k}\left(G_1 + \frac{T}{2}\right) \\ \hat{\tau}_{i,2}^k = \tau_i^k - \frac{\alpha_i^k}{1+\alpha_i^k}\left(G_2 + \frac{T}{2}\right). \end{cases} \quad (4)$$

Thus, the estimation of time delay $\hat{\tau}_i^k$ and Doppler factor $\hat{\alpha}_i^k$ are given by

$$\begin{cases} \hat{\alpha}_i^k = \dfrac{\hat{\tau}_{i,2}^k - \hat{\tau}_{i,1}^k}{G_1 - G_2 - \hat{\tau}_{i,2}^k + \hat{\tau}_{i,1}^k} \\ \hat{\tau}_i^k = \dfrac{1}{2}\left[\hat{\tau}_{i,1}^k + \hat{\tau}_{i,2}^k + \dfrac{\hat{\alpha}_i^k}{1+\hat{\alpha}_i^k}(G_1 + G_2 + T)\right]. \end{cases} \quad (5)$$

And then, the range measurement can be obtained by $\hat{d}_i^k = c\hat{\tau}_i^k$, and relative velocity measurement is $\hat{v}_i^k = c\hat{\alpha}_i^k$, based on the measuring signal from ith anchor.

It should be noted that the time delay estimation of HFM_1 and HFM_2 is independent of each other. $\hat{\tau}_{i,1}^k$ and $\hat{\tau}_{i,2}^k$ can be assumed to follow a Gaussian distribution with a variance σ^2, expressed as

$$\begin{cases} \hat{\tau}_{i,1}^k \sim \mathcal{N}\left(\tau_i^k - \frac{\alpha_i^k}{1+\alpha_i^k}(G_1 + T/2), \sigma^2\right) \\ \hat{\tau}_{i,2}^k \sim \mathcal{N}\left(\tau_i^k - \frac{\alpha_i^k}{1+\alpha_i^k}(G_2 + T/2), \sigma^2\right). \end{cases} \quad (6)$$

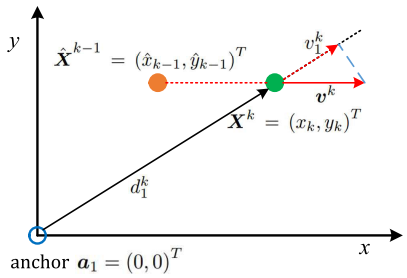

Fig. 4. Description of range and relative velocity-based localization.

With (4), the distribution of range measurements $\hat{d}_i^k$ and relative velocity measurements $\hat{v}_i^k$ can be given by

$$\begin{cases} \hat{v}_i^k \approx \mathcal{N}\left(v_i^k, 2\left(c\frac{1+\alpha_i^k}{G_1 - G_2}\sigma\right)^2\right) \\ \hat{d}_i^k \sim \mathcal{N}\left(d_i^k, \frac{1}{2}(c\sigma)^2\right) \end{cases} \quad (7)$$

where v_i^k is the truth value of $\hat{v}_i^k$, and d_i^k is the truth value of $\hat{d}_i^k$. Symbol "$\approx$" in the equation means that v_i^k approximately follows a Gaussian distribution. We can find that the variance of range measurements is decreased compared with ranging based on HFM_1 or HFM_2, which means higher ranging stability and precision. Meanwhile, the performance of relative velocity estimation could be improved by using a narrow measuring signal with a higher central frequency.

C. Theory of Rang and Relative Velocity-Based Localization

As depicted in Fig. 4, an anchor is deployed at position $\boldsymbol{a}_1$, while a smart device moves from position $\hat{\boldsymbol{X}}^{k-1}$ to $\boldsymbol{X}^k$ at time k. In the context of indoor localization, the accuracy of position has the highest priority. Therefore, we adopt a first-order motion model assumption, where the speed is approximated by using the assumption that the motion of the smart device between $\hat{\boldsymbol{X}}^{k-1}$ and $\boldsymbol{X}^k$ follows a uniform linear motion with a constant velocity $\boldsymbol{v}^k$. Here, $\hat{\boldsymbol{X}}^{k-1}$ represents the estimated position with a bias of $\boldsymbol{X}^{k-1}$ at time $k-1$.

Correspondingly, the observation of the smart device's velocity from the acoustic signal, denoted as v_1^k, represents the projection of $\boldsymbol{v}^k$ on the vector $(\boldsymbol{X}^k - \boldsymbol{a}_1)$. From another perspective, v_1^k contains partial information about the velocity $\boldsymbol{v}^k$, position $\boldsymbol{X}^k$ and $\hat{\boldsymbol{X}}^{k-1}$. By combining range measurements and relative velocity measurements, the position of the smart device can be determined.

The positions of anchors are definite and denoted as $\boldsymbol{a}_i = (a_{x,i}, a_{y,i})^T$, $i = 1, 2, \ldots, N$. At time k, The range measurement between smart device and ith anchor, $\hat{d}_i^k$, can be expressed as

$$\hat{d}_i^k = \|\boldsymbol{X}^k - \boldsymbol{a}_i\|_2 + \text{bias}_{i,d}^k + \epsilon_i^k = c\hat{\tau}_i^k \quad (8)$$

where $\hat{\tau}_i^k$ represents the TOA estimation from ith anchor, and ϵ_i^k denotes the error in range measurement. Specifically, $\text{bias}_{i,d}^k$ denotes a positive range bias of range measurement caused by NLOS. In addition, it is important to note that

$\text{bias}_{i,d}^k > 0$ during an NLOS condition, while $\text{bias}_{i,d}^k = 0$ under LOS conditions.

The relative velocity $\hat{v}_i^k$ can be obtained from the acoustic signal by estimating the Doppler-shift. The shift is calculated as

$$\begin{aligned}\hat{v}_i^k &= \frac{(\boldsymbol{v}^k)^T(\boldsymbol{X}^k - \boldsymbol{a}_i)}{\|\boldsymbol{X}^k - \boldsymbol{a}_i\|_2} + \text{bias}_{i,v}^k + \eta_i^k \\ &= c\left(\frac{\hat{f}_i^k}{f_0} - 1\right)\end{aligned} \tag{9}$$

where f_0 represents the original central frequency of acoustic signal, $\hat{f}_i^k$ stands for the estimated value of f_0, and η_i^k denotes the error in relative velocity measurement. Moreover, $\text{bias}_{i,v}^k$ represents a bias of relative velocity of measurement introduced by NLOS, and the magnitude of this bias depends on the geometry relationship among the smart devices, anchors, and blockers. $\text{bias}_{i,v}^k = 0$ while under LOS conditions.

Under the assumption of a first-order motion model for the moving target, where the measured interval between time $k-1$ and k is Δt, the estimation of $\boldsymbol{X}^k$, which is denoted as $\hat{\boldsymbol{X}}^k$, can be obtained by

$$\hat{\boldsymbol{X}}^k = \hat{\boldsymbol{X}}^{k-1} + \Delta t \boldsymbol{v}^k. \tag{10}$$

An LOS information matrix $\boldsymbol{l}^k$ is constructed to save the information of LOS measurements and eliminate the influence of NLOS measurements on the localization method. Consequently, the estimation of $\boldsymbol{X}^k$ using range and relative velocity measurements can be expressed as

$$\hat{\boldsymbol{X}}^k = F\left(\hat{\boldsymbol{X}}^{k-1}, \hat{d}_1^k, \ldots, \hat{d}_N^k, \hat{v}_1^k, \ldots, \hat{v}_N^k, \Delta t, \boldsymbol{l}^k\right). \tag{11}$$

In order to solve (11), we will introduce the maximum likelihood solution, least square solution and its closed-form solution. In addition, a new solution will be proposed by jointly estimating the positions in a short-time position sequence to break the error propagation and accumulation chain. Details of these solutions will be presented in the following sections, respectively.

D. Maximum Likelihood Solution

With the NLOS measurements discarded using the LOS information matrix $\boldsymbol{l}^k$, we can proceed to obtain a maximum likelihood estimator (MLE) solution for range and relative velocity-based localization. We assume that both range and relative velocity measurements follow Gaussian distribution, while the variances are $\sigma_{d,i,k}$ and $\sigma_{v,i,k}$, respectively. Specifically,

$$\epsilon_i^k \sim \mathcal{N}\left(0, \sigma_{d,i,k}^2\right), \eta_i^k \sim \mathcal{N}\left(0, \sigma_{v,i,k}^2\right), \quad i = 1, 2, \ldots, N. \tag{12}$$

The bias for LOS measurements is zero, represented as $\text{bias}_{i,d}^k = 0$ and $\text{bias}_{i,v}^k = 0$. As the NLOS measurements have been disregarded, their distribution can be treated as a uniform distribution. The distributions only depend on the uncertainty $\sigma_{d,i,k}$ and $\sigma_{v,i,k}$ regardless of the location of $\boldsymbol{X}^k$.

The range and relative velocity measurements between the receiver and the anchors are rewritten in a vector form, $\hat{\boldsymbol{D}}^k = \{\hat{d}_1^k, \hat{d}_2^k, \ldots, \hat{d}_N^k\}$, $\hat{\boldsymbol{V}}^k = \{\hat{v}_1^k, \hat{v}_2^k, \ldots, \hat{v}_N^k\}$. Correspondingly, the truth values of $\hat{\boldsymbol{D}}^k$ and $\hat{\boldsymbol{V}}^k$ are denoted as $\boldsymbol{D}^k = \{d_1^k, d_2^k, \ldots, d_N^k\}$ and $\boldsymbol{V}^k = \{v_1^k, v_2^k, \ldots, v_N^k\}$. At position $\boldsymbol{X}^k$, the joint probability density of $\hat{\boldsymbol{D}}^k$ and $\hat{\boldsymbol{V}}^k$ are given by

$$\begin{aligned}p\left(\hat{\boldsymbol{D}}^k; \boldsymbol{X}^k\right) &= \prod_{i=1}^{N} \frac{1}{\sqrt{2\pi\sigma_{d,i,k}^2}} \exp\left\{-\frac{\left[l_i^k\left(\hat{d}_i^k - d_i^k\right)\right]^2}{2\sigma_{d,i,k}^2}\right\} \\ &= \frac{1}{\sqrt{(2\pi)^N \det\left(\boldsymbol{Q}_{d,k}\right)}} \\ &\quad \cdot \exp\left\{-\frac{1}{2}\left(\hat{\boldsymbol{D}}^k - \boldsymbol{D}^k\right)^T \left(\boldsymbol{l}^k\right)^T \boldsymbol{Q}_{d,k}^{-1} \boldsymbol{l}^k \left(\hat{\boldsymbol{D}}^k - \boldsymbol{D}^k\right)\right\}\end{aligned} \tag{13}$$

$$\begin{aligned}p\left(\hat{\boldsymbol{V}}^k; \boldsymbol{X}^k\right) &= \prod_{i=1}^{N} \frac{1}{\sqrt{2\pi\sigma_{v,i,k}^2}} \exp\left\{-\frac{\left[l_i^k\left(\hat{v}_i^k - v_i^k\right)\right]^2}{2\sigma_{v,i,k}^2}\right\} \\ &= \frac{1}{\sqrt{(2\pi)^N \det\left(\boldsymbol{Q}_{v,k}\right)}} \\ &\quad \cdot \exp\left\{-\frac{1}{2}\left(\hat{\boldsymbol{V}}^k - \boldsymbol{V}^k\right)^T \left(\boldsymbol{l}^k\right)^T \boldsymbol{Q}_{v,k}^{-1} \boldsymbol{l}^k \left(\hat{\boldsymbol{V}}^k - \boldsymbol{V}^k\right)\right\}\end{aligned} \tag{14}$$

where l_i^k represents the LOS information of the measurements from the ith anchor, $l_i^k = 1$ for LOS measurements while $l_i^k = 0$ for NLOS measurements; $\boldsymbol{l}^k = \text{diag}\{l_1^k, l_2^k, \ldots, l_N^k\}$ is the LOS information matrix at time k; $\det(\cdot)$ is the determination operator; $\boldsymbol{Q}_{d,k}$ and $\boldsymbol{Q}_{v,k}$ are the auto-covariance matrix of $\boldsymbol{\epsilon}^k$ and $\boldsymbol{\eta}^k$, respectively, and given by

$$\boldsymbol{Q}_{d,k} = E\left\{\boldsymbol{\epsilon}^k \left(\boldsymbol{\epsilon}^k\right)^T\right\} = \text{diag}\left\{\sigma_{d,1,k}^2, \ldots, \sigma_{d,N,k}^2\right\} \tag{15}$$

$$\boldsymbol{Q}_{v,k} = E\left\{\boldsymbol{\eta}^k \left(\boldsymbol{\eta}^k\right)^T\right\} = \text{diag}\left\{\sigma_{v,1,k}^2, \ldots, \sigma_{v,N,k}^2\right\}. \tag{16}$$

$\boldsymbol{\epsilon}^k = [\epsilon_1^k, \ldots, \epsilon_N^k]^T$ and $\boldsymbol{\eta}^k = [\eta_1^k, \ldots, \eta_N^k]^T$ are the vector form of range measurements and relative velocity measurements.

By using (13) and (14), the estimation of $\boldsymbol{X}^k$ based on range and relative velocity can be given by

$$\hat{\boldsymbol{X}}^k = \arg\max_{\boldsymbol{X}^k} p\left(\hat{\boldsymbol{D}}^k, \hat{\boldsymbol{V}}^k; \boldsymbol{X}^k\right). \tag{17}$$

Based on the independence assumption, we have

$$p\left(\hat{\boldsymbol{D}}^k, \hat{\boldsymbol{V}}^k; \boldsymbol{X}^k\right) = p\left(\hat{\boldsymbol{D}}^k; \boldsymbol{X}^k\right) p\left(\hat{\boldsymbol{V}}^k; \boldsymbol{X}^k\right). \tag{18}$$

Then, (17) is equivalent to

$$\begin{aligned}\hat{\boldsymbol{X}}^k = \arg\min_{\boldsymbol{X}^k} \Big\{&\left(\hat{\boldsymbol{V}}^k - \boldsymbol{V}^k\right)^T \left(\boldsymbol{l}^k\right)^T \boldsymbol{Q}_{v,k}^{-1} \boldsymbol{l}^k \left(\hat{\boldsymbol{V}}^k - \boldsymbol{V}^k\right) \\ &+ \left(\hat{\boldsymbol{D}}^k - \boldsymbol{D}^k\right)^T \left(\boldsymbol{l}^k\right)^T \boldsymbol{Q}_{d,k}^{-1} \boldsymbol{l}^k \left(\hat{\boldsymbol{D}}^k - \boldsymbol{D}^k\right)\Big\}.\end{aligned} \tag{19}$$

Given that d_i^k and v_i^k are nonlinear functions by $\boldsymbol{X}^k$, as indicated in (8) and (9), (19) can be addressed by using a grid search method in the solution space with sufficiently dense grid points. However, $\boldsymbol{Q}_{d,k}$ and $\boldsymbol{Q}_{v,k}$ are very difficult to estimate in real applications because the limited update frequency of acoustic indoor localization technology makes it challenging to gather sufficient measurements for statistical analysis within a short time. Therefore, a weighted least square method is used instead of maximum likelihood estimation to estimate the positions.

E. Least Square Solution and its Closed-Form Solution

Referring to (19), the solution based on the least square estimator (LSE) can be given as

$$\hat{\boldsymbol{X}}^k = \arg\min_{\boldsymbol{X}^k} J\left(\boldsymbol{X}^k\right) \tag{20}$$

where the cost function $J(\boldsymbol{X}^k)$ is

$$J\left(\boldsymbol{X}^k\right) = \sum_{i=1}^{N}\left\{\beta_{d,i}^k\left(\hat{d}_i^k - d_i^k\right)^2 + \beta_{v,i}^k\left(\hat{v}_i^k - v_i^k\right)^2\right\}. \tag{21}$$

The weight coefficients $\beta_{d,i}^k$ and $\beta_{v,i}^k$ denote the reliability of range and relative velocity measurements from each anchor. By setting $\beta_{d,i}^k = l_i^k/\sigma_{d,i,k}^2$ and $\beta_{v,i}^k = l_i^k/\sigma_{v,i,k}^2$, (21) is equivalent to (19).

In practical applications, obtaining prior knowledge of measurement errors is often difficult. Therefore, a direct approach is to set $\beta_{d,i}^k = \beta_{v,i}^k = l_i^k$. Equation (21) could be calculated by using a grid search method in the solution space. In order to enhance computational efficiency, it is necessary to derive a closed-form solution of LSE. Initially, we will consider a closed-form solution of range and relative velocity-based localization problems under an LOS scenario and then derive the closed-form solution of LSE in an NLOS scenario.

For the LOS localization scenario, from Fig. 4, we can obtain the following relations:

$$\begin{cases} d_i = \left\|\boldsymbol{X}^k - \boldsymbol{a}_i\right\|_2 \\ v_i = \dfrac{\left(\boldsymbol{v}^k\right)^T\left(\boldsymbol{X}^k - \boldsymbol{a}_i\right)}{\left\|\boldsymbol{X}^k - \boldsymbol{a}_i\right\|_2} \end{cases}, \quad i = 1, 2, \ldots, N. \tag{22}$$

To rewrite the relative velocity equations in a vector form, we will obtain

$$\begin{aligned} \left(\boldsymbol{v}^k\right)^T\left(\boldsymbol{X}^k\boldsymbol{I}_{1\times N} - \boldsymbol{A}\right) &= \boldsymbol{B}_k \\ \boldsymbol{A} &= [\boldsymbol{a}_1, \boldsymbol{a}_2, \ldots, \boldsymbol{a}_N] \\ \boldsymbol{B}_k &= \left[d_1^k v_1^k, d_2^k v_2^k, \ldots, d_N^k v_N^k\right]^T \end{aligned} \tag{23}$$

where $\boldsymbol{I}_{1\times N}$ denotes a $1 \times N$ identity matrix. Based on (23), we can obtain

$$\left(\boldsymbol{v}^k\right)^T = \boldsymbol{B}_k\left(\boldsymbol{X}^k\boldsymbol{I}_{1\times N} - \boldsymbol{A}\right)^{\dagger} \tag{24}$$

where "†" is the pseudo-inverse operator. Then, $\boldsymbol{X}^k$ can be given by

$$\boldsymbol{X}^k = \hat{\boldsymbol{X}}^{k-1} + \Delta t\left(\boldsymbol{B}_k\left(\boldsymbol{X}^k\boldsymbol{I}_{1\times N} - \boldsymbol{A}\right)^{\dagger}\right)^T. \tag{25}$$

Equation (25) can be reformed and expanded as

$$\begin{aligned} \boldsymbol{I}_{N\times 1}\left(\boldsymbol{X}^k\right)^T\boldsymbol{X}^k - \boldsymbol{A}^T\boldsymbol{X}^k = \boldsymbol{I}_{N\times 1}\left(\boldsymbol{X}^k\right)^T\hat{\boldsymbol{X}}^{k-1} \\ -\boldsymbol{A}^T\hat{\boldsymbol{X}}^{k-1} + \Delta t\boldsymbol{B}_k^T. \end{aligned} \tag{26}$$

Range calculation equation in (22) can be rewritten and expanded as

$$\left(\boldsymbol{X}^k\right)^T\boldsymbol{X}^k - 2\boldsymbol{a}_i^T\boldsymbol{X}^k = d_i^2 - \boldsymbol{a}_i^T\boldsymbol{a}_i, \quad i = 1, 2, \ldots, N. \tag{27}$$

Then, to transform this equation into a vector form, we can obtain

$$\begin{aligned} \boldsymbol{I}_{N\times 1}\left(\boldsymbol{X}^k\right)^T\boldsymbol{X}^k - 2\boldsymbol{A}^T\boldsymbol{X}^k &= \boldsymbol{d}_k - \boldsymbol{A}_m \\ \boldsymbol{d}_k &= \left[\left(d_1^k\right)^2, \left(d_2^k\right)^2, \ldots, \left(d_N^k\right)^2\right]^T \\ \boldsymbol{A}_m &= \left[\boldsymbol{a}_1^T\boldsymbol{a}_1, \boldsymbol{a}_2^T\boldsymbol{a}_2, \ldots, \boldsymbol{a}_N^T\boldsymbol{a}_N\right]^T. \end{aligned} \tag{28}$$

Therefore, based on (26) and (28), the closed-form solution of the basic LSE method in LOS scenario can be expressed as

$$\begin{aligned} \hat{\boldsymbol{X}}^k = &\left[\left(\boldsymbol{A} - \hat{\boldsymbol{X}}^{k-1}\boldsymbol{I}_{1\times N}\right)\left(\boldsymbol{A} - \hat{\boldsymbol{X}}^{k-1}\boldsymbol{I}_{1\times N}\right)^T\right]^{-1} \\ &\times\left(\boldsymbol{A} - \hat{\boldsymbol{X}}^{k-1}\boldsymbol{I}_{1\times N}\right)\left(\Delta t\boldsymbol{B}_k^T + \boldsymbol{A}_m - \boldsymbol{d}_k - \boldsymbol{A}^T\hat{\boldsymbol{X}}^{k-1}\right). \end{aligned} \tag{29}$$

In particular, it needs to be noted that when there is only one anchor available for position estimation, that is $N = 1$, (29) is expressed as

$$\begin{aligned} \hat{\boldsymbol{X}}^k = &\left[\left(\boldsymbol{a}_1 - \hat{\boldsymbol{X}}^{k-1}\right)\left(\boldsymbol{a}_1 - \hat{\boldsymbol{X}}^{k-1}\right)^T\right]^{-1} \\ &\times\left(\boldsymbol{a}_1 - \hat{\boldsymbol{X}}^{k-1}\right)\left(\Delta t d_1^k v_1^k + \boldsymbol{a}_1^T\boldsymbol{a}_1 - \left(d_1^k\right)^2 - \boldsymbol{a}_1^T\hat{\boldsymbol{X}}^{k-1}\right). \end{aligned} \tag{30}$$

Clearly, the matrix $(\boldsymbol{a}_1 - \hat{\boldsymbol{X}}^{k-1})(\boldsymbol{a}_1 - \hat{\boldsymbol{X}}^{k-1})^T$ is singular, indicating a lack of uniqueness in the solution for $\hat{\boldsymbol{X}}^k$ when $N = 1$. The condition for ensuring the LSE has a unique solution is $N \geq 2$ for 2-D positioning and $N \geq 3$ for 3-D positioning.

Then, based on (29), the closed-form solution of LSE in the NLOS scenario can be written and simplified as

$$\begin{aligned} \hat{\boldsymbol{X}}^k = &\left[\left(\boldsymbol{A} - \hat{\boldsymbol{X}}^{k-1}\boldsymbol{I}_{1\times N}\right)\boldsymbol{l}^k\left(\boldsymbol{A} - \hat{\boldsymbol{X}}^{k-1}\boldsymbol{I}_{1\times N}\right)^T\right]^{-1} \\ &\times\left(\boldsymbol{A} - \hat{\boldsymbol{X}}^{k-1}\boldsymbol{I}_{1\times N}\right)\boldsymbol{l}^k\left(\Delta t\boldsymbol{B}_k^T + \boldsymbol{A}_m - \boldsymbol{d}_k - \boldsymbol{A}^T\hat{\boldsymbol{X}}^{k-1}\right). \end{aligned} \tag{31}$$

F. Supplementing Strategy for Insufficient LOS Measurements

In (31), the rank of the term needed to be inverted should be greater than the dimension of position to make the LSE has a unique solution, that is,

$$\|\boldsymbol{l}^k\|_2 \geq D_p \tag{32}$$

where D_p represents the dimension of position space, while $D_p = 2$ indicates a 2-D position space and $D_p = 3$ represents a 3-D position space. Equation (32) is also the condition for making (19) to have a unique solution.

For the purpose of mitigating the limitations in LOS measurements under dense NLOS environments, an insufficient LOS measurement supplementing strategy can be employed. This involves selecting a number of NLOS anchors with the shorter range measurements and treating them as LOS anchors, ensuring that condition (32) is upheld.

Based on the principles of indoor geometric acoustics theory [36], it can be inferred that shorter NLOS propagation paths result in signals that undergo fewer reflections, experience less energy absorption, and are consequently more likely to exhibit lower ranging errors. By designating these shorter NLOS propagation paths as the LOS paths, the supplementing strategy for insufficient LOS measurements could minimize the impact of NLOS measurements on the accuracy of positioning results.

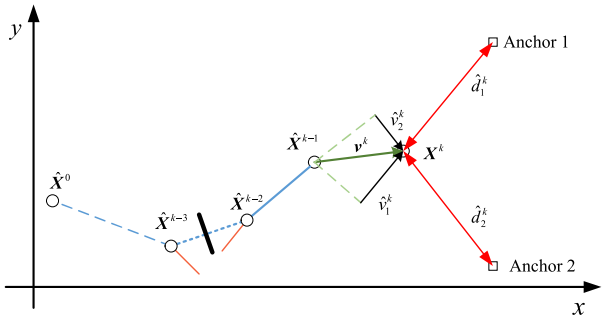

Fig. 5. Localization process of range and relative velocity-based localization.

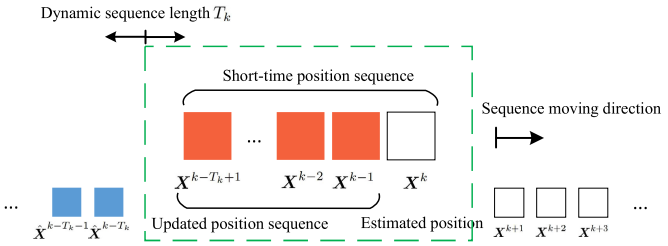

Fig. 6. Principle of the proposed MPJE method.

G. Error Accumulation Analysis

Through (11) and (31), we can find that the estimation error of $\boldsymbol{X}^k$, denoted as $\boldsymbol{\xi}^k$, depends on $\boldsymbol{\xi}^{k-1}$, $\boldsymbol{\epsilon}^k$, and $\boldsymbol{\eta}^k$. That is,

$$\boldsymbol{\xi}^k = h\left(\boldsymbol{\xi}^{k-1}, \boldsymbol{\epsilon}^k, \boldsymbol{\eta}^k\right). \tag{33}$$

The range measurement error $\boldsymbol{\epsilon}^k$ and relative velocity measurement error $\boldsymbol{\eta}^k$ can enter the whole calculation cycle by influencing the positioning error $\boldsymbol{\xi}^k$, as $\boldsymbol{\xi}^k$ can directly influence $\boldsymbol{\xi}^{k+1}$ at time $k+1$. The positioning error will accumulate rapidly over time, deteriorating the performance of the system. This process could be illustrated by Fig. 5.

Unlike the conventional range-based localization, the introduction of velocity measurements makes the positioning process no longer uncorrelated to each other. Conversely, the positions estimation of adjacent times is related to each other, forming a "chain" as shown in Fig. 5. Estimating $\boldsymbol{X}^k$ depends on the estimation of $\boldsymbol{X}^{k-1}$. As a result, errors propagate and accumulate rapidly along this "chain." To improve the localization performance of the range and relative velocity-based localization method, it is crucial to find ways to break the chain of error propagation. In this article, an MPJE method is going to be proposed to solve this problem.

III. Multiposition Joint Estimation

Breaking the error propagation chain will split the localization process into many small pieces, as shown in Fig. 5. These small pieces are named as the "short-time position sequence" in this article. If the positions in sequence $\{\boldsymbol{X}^{k-2}, \boldsymbol{X}^{k-1}, \boldsymbol{X}^k\}$ could be independently estimated, the influence of position bias of $\boldsymbol{X}^{k-3}$ on $\boldsymbol{X}^{k-2}$ can be eliminated. Thus, an MPJE method is proposed to mitigate the influence of $\boldsymbol{\epsilon}^k$ and $\boldsymbol{\eta}^k$ in (33) by jointly estimating the positions in each short-time position sequence.

A. Algorithm Architecture

The proposed MPJE method for range and relative velocity-based localization, which is named as MPJE, is a nonlinear weighted least square problem with a length of short-time position sequence T_k. The principle behind the proposed method is shown in Fig. 6. The core idea of our method is to cover insufficient LOS measurements for a single position estimation by utilizing the LOS measurements redundancy in the sequence since adjacent positions are connected by velocity measurements. At the same time, considering the position estimation of the sequence as an independent process can break the error propagation chain prior to the sequence.

As depicted in Fig. 6, $\boldsymbol{X}^k$ represents the position to be estimated at time k. The short-time position sequence, denoted as $\{\boldsymbol{X}^{k-T_k+1}, \boldsymbol{X}^{k-T_k+2}, \ldots, \boldsymbol{X}^{k-1}, \boldsymbol{X}^k\}$ is jointly estimated by our proposed MPJE method. This sequence has a length of T_k and it is worth mentioning that all positions from between $k-1$ to time $k-T_k+1$ are recalculated and updated. Thus, the sequence $\{\boldsymbol{X}^{k-T_k+1}, \boldsymbol{X}^{k-T_k+2}, \ldots, \boldsymbol{X}^{k-1}\}$ is referred to as "updated positions sequence." Notably, $\boldsymbol{X}^{k-T_k+1}$ is the "starting position" of the sequence, which is considered as unknown and estimated along with the other locations. By releasing the initial position of the velocity integral process, the propagation chain of the relative velocity error can be broken. The influence of $\boldsymbol{\epsilon}^k$ and $\boldsymbol{\eta}^k$ can be greatly mitigated.

The short-time position sequence moves along with the direction of increasing k. The dynamic sequence length T_k is adjusted based on the LOS measurements redundancy of the sequence. When the LOS measurements redundancy of sequence is a surplus, T_k decreases, and when there is insufficient redundancy, T_k increases. In this way, the indoor localization problem in dense NLOS environments can be tackled in the real world. It is found that only two LOS anchors are required for accurate localization, although allowing for one LOS anchor for a short period of time is acceptable.

To summarize, in our proposed MPJE method, the error propagation chain is cut off by the short-time position sequence estimation, and the insufficient LOS measurements for accurate localization introduced by the dense NLOS environments are supplemented by extending the length of the short-time position sequence to increase the LOS measurements redundancy.

B. Mathematical Model

The modeling of the joint estimation process for the short-time sequence $\{\boldsymbol{X}^{k-T_k+1}, \boldsymbol{X}^{k-T_k+2}, \ldots, \boldsymbol{X}^k\}$ is an "extension" of LS method in (20), and the new nonlinear weighted least square problem can be expressed as

$$\hat{\boldsymbol{X}}^{k-T_k+1}, \hat{\boldsymbol{X}}^{k-T_k+2}, \ldots, \hat{\boldsymbol{X}}^k = \arg \min_{\boldsymbol{X}^{k-T_k+1}, \ldots, \boldsymbol{X}^k} \frac{1}{2} (\boldsymbol{LWE})^T (\boldsymbol{LWE}) \tag{34}$$

where

$$\boldsymbol{E} = \left[\boldsymbol{e}_d^{k-T_k+1}, \boldsymbol{e}_d^{k-T_k+2}, \boldsymbol{e}_v^{k-T_k+2}, \ldots, \boldsymbol{e}_d^k, \boldsymbol{e}_v^k\right]^T$$

$$
\begin{aligned}
\boldsymbol{W} &= \mathrm{diag}\left\{\boldsymbol{w}_d^{k-T_k+1}, \boldsymbol{w}_d^{k-T_k+2}, \boldsymbol{w}_v^{k-T_k+2}, \ldots, \boldsymbol{w}_d^{k}, \boldsymbol{w}_v^{k}\right\} \\
\boldsymbol{L} &= \mathrm{diag}\left\{\boldsymbol{l}_d^{k-T_k+1}, \boldsymbol{l}^{k-T_k+2}, \boldsymbol{l}^{k-T_k+2}, \ldots, \boldsymbol{l}^{k}, \boldsymbol{l}^{k}\right\} \\
\boldsymbol{w}_d^k &= \mathrm{diag}\left\{w_{d,1}^k, w_{d,2}^k, \ldots, w_{d,N}^k\right\} \\
\boldsymbol{w}_v^k &= \mathrm{diag}\left\{w_{v,1}^k, w_{v,2}^k, \ldots, w_{v,N}^k\right\} \\
\boldsymbol{l}^k &= \mathrm{diag}\left\{l_1^k, l_2^k, \ldots, l_N^k\right\} \\
\boldsymbol{e}_d^k &= \left[\hat{d}_1^k - d_1^k, \hat{d}_2^k - d_2^k, \ldots, \hat{d}_N^k - d_N^k\right] \\
\boldsymbol{e}_v^k &= \left[\hat{v}_1^k - v_1^k, \hat{v}_2^k - v_2^k, \ldots, \hat{v}_N^k - v_N^k\right].
\end{aligned} \tag{35}
$$

In the equations, $\boldsymbol{E}$ represents the errors vector, $\boldsymbol{W}$ corresponds to the weight matrix, and $\boldsymbol{L}$ denotes the LOS information matrix. On the other hand, $\boldsymbol{w}_d^k$ and $\boldsymbol{w}_v^k$ refer to the range weight matrix and relative velocity weight matrix, respectively. The values of both matrices can be adjusted to modify the impact of range and relative velocity measurements on localization results.

For sequence $\{\boldsymbol{X}^{k-T_k+1}, \boldsymbol{X}^{k-T_k+2}, \ldots, \boldsymbol{X}^k\}$, a total of T_k positions need to be estimated. This implies the number of unknown variables is $D_p T_k$, where D_p represents the spatial dimension of positions. Similar to condition (32), the condition of (34) having a unique solution is to make sure that the rank of $\boldsymbol{E}\boldsymbol{E}^T$ is greater than $D_p T_k$. The difference is that the LOS measurements redundancy R_k is introduced to quantify it as a metric. R_k is given by

$$
R_k = 2\sum_{t=1}^{T_k} \left|\boldsymbol{l}^{k-t+1}\right| - \left|\boldsymbol{l}^{k-T_k+1}\right| - D_p T_k. \tag{36}
$$

For the LOS localization scenario with two anchors, that is $N = 2$, the redundancy $R_k = 2$ while $T_k = 2$. The redundancy of LOS measurements could greatly improve the localization precision. R_k increases with T_k. In comparison to conventional localization methods, the required number of LOS anchors has been reduced from 3 to 2, resulting in a substantial reduction in system deployment costs. In addition, (36) indicates that the quantity of LOS anchors necessary for accurate localization has been relaxed.

For example, in a dense NLOS environment, the number of LOS anchors from time $k-3$ to k is given by the sequence $\{2, 1, 1, 2\}$. In this condition, the redundancy $R_k = 2$, and we can still achieve accurate localization based on (34). Therefore, in dense NLOS localization scenarios, it is possible to achieve accurate localization even when only one LOS anchor is available at certain times using the proposed method.

The problem in (34) is actually a high dimensional weighted nonlinear least square problem. The commonly used linearization method based on Taylor expansion generally exhibits poor calculation accuracy. To enhance the calculation accuracy of the solution, iterative optimization algorithms, such as the fastest descent method, the Gauss–Newton method, and the LM algorithm, are employed for rapid solution computation. The LM algorithm, compared to the other two methods, exhibits the characteristics of local convergence similar to the Gauss–Newton method and global convergence similar to the fastest descent method. It is an effective tool for solving nonlinear least square [37]. Therefore, we utilize the LM algorithm as proposed in [38], to solve the high dimensional weighted nonlinear least square problem presented in (34).

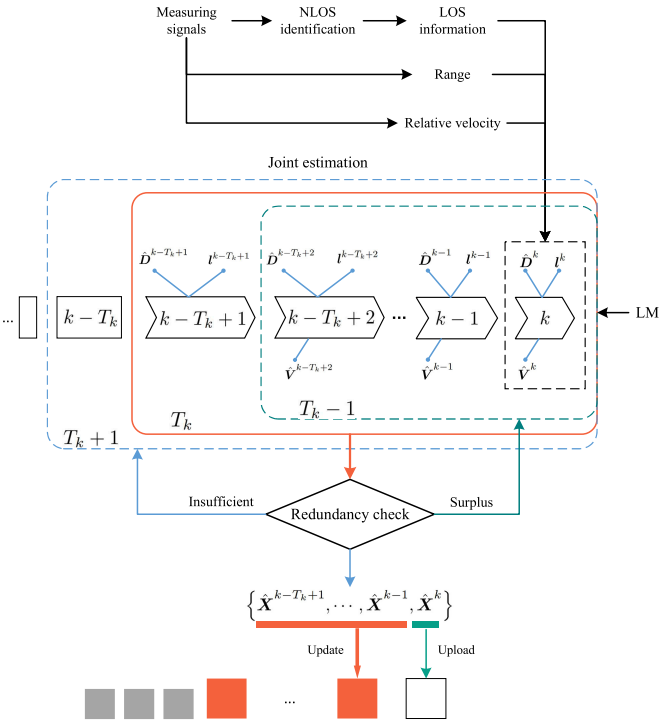

Fig. 7. Architecture of the proposed MPJE method.

C. Algorithm

The architecture of the proposed MPJE method is designed based on the principle shown in Fig. 6 and illustrated in Fig. 7. The NLOS identification is performed based on the received signals using the method proposed in [20]. Subsequently, the LOS information matrix $\boldsymbol{l}^k$ is constructed. The range and relative velocity measurements $\hat{\boldsymbol{D}}^k$ and $\hat{\boldsymbol{V}}^k$ are obtained by using (22). The NLOS measurements in $\hat{\boldsymbol{D}}^k$ and $\hat{\boldsymbol{V}}^k$ are discarded by $\boldsymbol{l}^k$.

The starting position of the short-time position sequence, $\boldsymbol{X}^{k-T_k+1}$, is used for the MPJE by only considering the range measurements $\hat{\boldsymbol{D}}^{k-T_k+1}$ excluding the relative velocity measurements $\hat{\boldsymbol{V}}^{k-T_k+1}$, in order to cut off the error propagation chain from time $k-T_k$ to time $k-T_k+1$.

The MPJE is performed using a weighted nonlinear least square method, which is efficiently calculated by the LM algorithm, to estimate the positions in the short-time position sequence simultaneously. The core of the LM algorithm is to construct a Jacobian matrix and a Hessian matrix. However, with the increase of the sequence length T_k, the dimensions of the two kinds of matrices will increase rapidly, leading to a sharp increase in memory consumption and calculation complexity. As a result, this increase in dimensions significantly raises power consumption and system application costs. Therefore, selecting an appropriate sequence length is recommended. In addition, the selection of the initial position in the iterative searching process of the LM algorithm is crucial for accelerating convergence and enhancing the accuracy of the estimation results.

The sequence length T_k is determined through a redundancy check process. If there is an excess in the LOS measurements redundancy R_k, the sequence should be reduced by $T_k - 1$. Conversely, the sequence should be extended by $T_k + 1$. To regulate this process, a threshold R_{thd} is introduced, and the process is given as

$$\begin{cases} \text{if } R_k > R_{\text{thd}}, & T_k - - \\ \text{if } R_k < R_{\text{thd}}, & T_k + +. \end{cases} \tag{37}$$

This method allows for reducing excess LOS measurements by shrinking the sequence length T_k, consequently decreasing the computational cost. On the other hand, extending T_k supplements insufficient LOS measurements, enhancing the accuracy of position estimation. Typically, a value of $R_{\text{thd}} = 4$ or 6 is empirically set to balance calculation cost and localization precision.

To improve the mean localization precision, it is important to limit the number of LOS anchors at time k to D_p+1, that is, $|\boldsymbol{l}^k| \leq D_p+1$. According to the condition in (32), the minimum number of LOS anchors required for a unique solution has been reduced to D_p. From the results of experiments, we found it out that the increase of $|\boldsymbol{l}^k|$ does not lead to significant performance improvement, but it does increase the calculation cost of LM when $|\boldsymbol{l}^k| \leq D_p + 1$. In addition, limiting the value of $|\boldsymbol{l}^k|$ also serves to protect the estimation performance of the sequence, thereby giving more attention to measurement points with fewer NLOS measurements.

The LM algorithm is an iterative searching process where the initial searching positions $\boldsymbol{X}_{\text{init}}$ play a critical role in accelerating convergence and improving the accuracy of estimation results. The initial search position is determined based on the historical estimation results $\{\hat{\boldsymbol{X}}^{k-t+1}; t = 1, 2, \ldots, T_k\}$, and is uploaded as $\boldsymbol{X}_{\text{init}} = \{\hat{\boldsymbol{X}}^{k-T_k+1}, \ldots, \hat{\boldsymbol{X}}^{k-1}, \check{\boldsymbol{X}}^k\}$. The prediction of $\boldsymbol{X}^k$, denoted as $\check{\boldsymbol{X}}^k$, is obtained through a linear prediction process

$$\check{\boldsymbol{X}}^k = 2\hat{\boldsymbol{X}}^{k-1} - \hat{\boldsymbol{X}}^{k-2}. \tag{38}$$

The outputs of the LM algorithm are the estimation results of the short-time position sequence at time k, denoted as $\{\hat{\boldsymbol{X}}_k^{k-t+1}; t = 1, 2, \ldots, T_k\}$. The final estimation results of our proposed MPJE method are obtained by an updating process to further improve the estimation precision, which is shown as follows:

$$\begin{aligned} \hat{\boldsymbol{X}}^k &\leftarrow \hat{\boldsymbol{X}}_k^k, \\ \hat{\boldsymbol{X}}^{k-t+1} &\leftarrow \frac{\hat{\boldsymbol{X}}^{k-t+1} + \hat{\boldsymbol{X}}_k^{k-t+1}}{2}, \quad t = 2, \ldots, T_k. \end{aligned} \tag{39}$$

At last, the detailed calculation process of our proposed MPJE method is shown in Algorithm 1.

Algorithm 1 MPJE Algorithm

Input: R_{thd}, T_{min}, T_{max}, Δt, $\hat{\boldsymbol{D}}^{k-T_{max}+1}, \ldots, \hat{\boldsymbol{D}}^k$, $\hat{\boldsymbol{V}}^{k-T_{max}+1}, \ldots, \hat{\boldsymbol{V}}^k$, $\boldsymbol{l}^{k-T_{max}+1}, \ldots, \boldsymbol{l}^k$;
Output: $\hat{\boldsymbol{X}}^k, \hat{\boldsymbol{X}}^{k-1}, \ldots, \hat{\boldsymbol{X}}^{k-T_k+1}$;
Set $T_k \leftarrow T_min$;
Upload $\boldsymbol{L}$, $\boldsymbol{W}$ and $\boldsymbol{E}$;
$R_k \leftarrow 2\sum_{t=1}^{T_k}\left|\boldsymbol{l}^{k-t+1}\right| - \left|\boldsymbol{l}^{k-T_k+1}\right| - D_p T_k$;
repeat
  Find the index i of the largest $\hat{d}_i^k$ in $\hat{\boldsymbol{D}}^k \odot \left(1 - \boldsymbol{l}^k\right)$, where $\odot$ is the operator of Hadamard product;
  $l_i^k \leftarrow 0$;
until $\left|\boldsymbol{l}^k\right| \leq D_p + 1$
if $R_k > R_{thd}$ **then**
  $T_k \leftarrow \max\{T_{min}, T_k - 1\}$;
end if
repeat
  $T_k \leftarrow \min\{T_{max}, T_k + 1\}$;
  $R_k \leftarrow 2\sum_{t=1}^{T_k}\left|\boldsymbol{l}^{k-t+1}\right| - \left|\boldsymbol{l}^{k-T_k+1}\right| - D_p T_k$;
until $R_k \geq R_{thd}$ or $T_k = T_{max}$
if $k \leq T_k$ **then**
  $\boldsymbol{X}_{init} \leftarrow$ random values;
else
  $\boldsymbol{X}_{init} \leftarrow \left\{\hat{\boldsymbol{X}}^{k-T_k+1}, \ldots, \hat{\boldsymbol{X}}^{k-1}, \check{\boldsymbol{X}}^k\right\}$;
end if
Solve (34) based on LM algorithm and obtain $\left\{\hat{\boldsymbol{X}}_k^{k-t+1}; t = 1, 2, \ldots, T_k\right\}$;
Updating the estimation of each positions based on (39);
return $\hat{\boldsymbol{X}}^k, \hat{\boldsymbol{X}}^{k-1}, \ldots, \hat{\boldsymbol{X}}^{k-T_k+1}$

IV. Numerical Simulations

The simulations have been realized using MATLAB and run on a computer with a 3.2 GHz 4-core processor and 16 G RAM. It is noteworthy that the memory required for simulations is less than 3 MB, making it compatible with any commercial personal computer. A basic NLOS localization scenario is constructed for numerical simulations to evaluate the performance of our proposed LSE and MPJE methods, as shown in Fig. 8. The size of the room is 40 × 30 m. A target follows a predetermined trajectory moving around a blocker from $(28, 17)^T$ (m) to $(28, 10)^T$ (m), $(22, 5)^T$ (m), $(14, 5)^T$ (m), $(14, 20)^T$ (m), and $(28, 21)^T$ (m) with a speed 1 m/s, and the position update frequency is 1 Hz. Four anchors and three blockers are deployed in the scenario to imitate a dense NLOS localization environment. The coordinates of the anchors, in order, are $\{(2, 2)^T, (38, 2)^T, (38, 28)^T, (2, 28)^T\}$ (m).

The number of LOS anchors varies with the target position. In Fig. 8, the positions that can receive signals from three LOS anchors are represented by the symbol ⋄, positions with two LOS anchors are marked with the symbol ∘, and positions with one LOS anchor are marked with the symbol ∗.

In addition, the target's motion trajectory encompasses rectilinear, curvilinear, and quarter-turning motions, thereby simulating realistic target maneuvers. Subsequently, the performance of LSE and MPJE is evaluated based on range and relative velocity in the LOS and NLOS scenarios, respectively. Selection of T_k and R_{thd} is investigated with respect to algorithm time cost and localization precision analysis. Finally, the influence of measurement noise on the localization performance is investigated and analyzed.

As a comparison, the PF method and Rauch–Tung–Striebel (RTS) smoothing method [39] are introduced to demonstrate the performance of our proposed MPJE method. The RTS

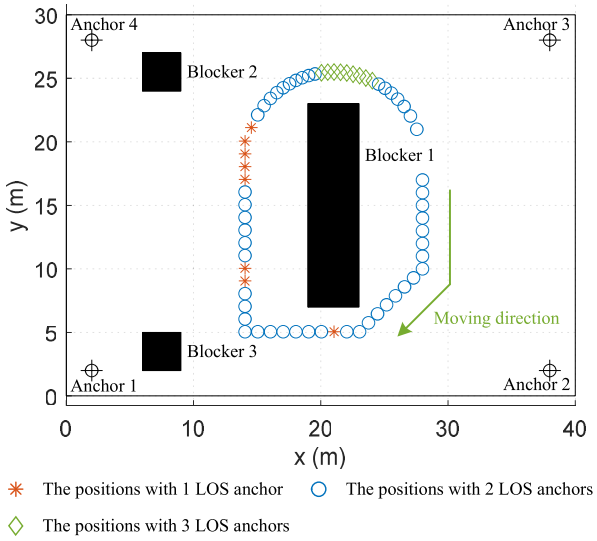

Fig. 8. Basic NLOS localization scenario.

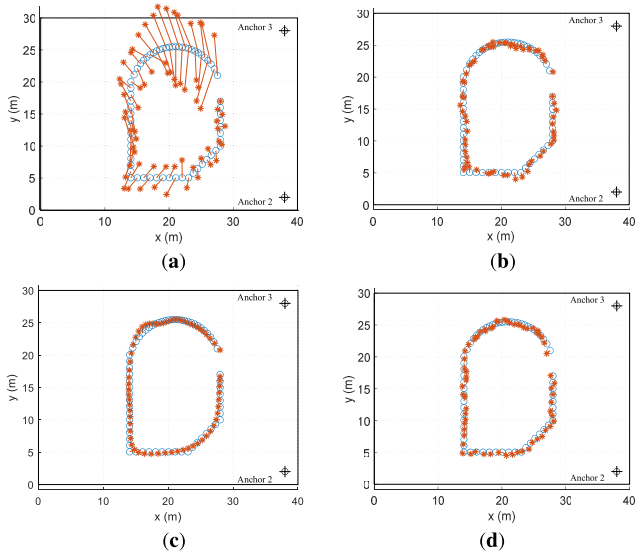

Fig. 9. LOS localization results based on different methods. (a) Closed-form LSE. (b) LSE. (c) LSE-RTS. (d) MPJE.

smoother is used to improve the LSE results, named as LSE-RTS.

A. Performance Evaluation in LOS Environments

Based on the scenario illustrated in Fig. 8, we have investigated and analyzed the performance of several methods: range measurements based MLE (denoted as MLE-R for short), range and relative velocity measurements based LSE, closed-form LSE, LSE-RTS, PF, and MPJE. This analysis is conducted in the LOS scenario by removing the blockers.

To emphasize the performance differences between the methods, we simulated a low anchor density using only two anchors. The standard deviations of range and relative velocity measurements are $\sigma_{d,i,k} = 0.5$ and $\sigma_{v,i,k} = 0.3$, respectively, where $i = 1, 2$. These values indicate that there is an 85% probability of the measurement errors being within ± 0.72 m and ± 0.43 m/s. Such noise pollution is significant for a velocity $v = 1$ m/s.

In addition, it is worth noting that there is no such unique solution for the MLE-R method when only two anchors are deployed. Artificial selection is required to ensure the selection of a feasible solution. In practical applications, this problem can be solved by restricting the search area for feasible solutions. Thus, for MLE based on range measurements, the search range of x^k is confined to the interval $[0, 40]$ (m), while y^k is limited to $[0, 30]$ (m). The sequence length and LOS measurements redundancy threshold in the MPJE method is set as $T_k = 4$ and $R_{\text{thd}} = 6$, respectively, with the weight matrix being set as $\boldsymbol{w}_d^k = \boldsymbol{w}_v^k$. The localization results are presented in Fig. 9.

Compared to other methods, the LSE closed-form method based on range and relative velocity measurements performs the worst. The accumulation of measurement errors can be clearly observed in Fig. 9(a). This phenomenon is not observed in the LSE method, as shown in Fig. 9(b), because the numerical search method in the solution space could greatly improve the positioning precision when there are sufficient LOS measurements. And the performance of LSE can be further improved by using the RTS smoother. The performance of LSE-RTS is higher than that of MPJE in this condition.

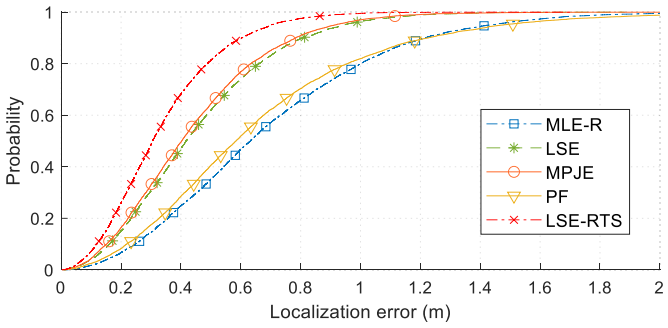

Fig. 10. CDF of the localization errors in the LOS scenario with $\sigma_{d,i,k} = 0.5$, $\sigma_{v,i,k} = 0.3$, and two anchors.

By repeating the simulation 1000 times, the cumulative distribution function (cdf) of the localization errors is investigated and plotted in Fig. 10. Since the localization precision of the LSE closed-form method is low, the following simulations focus on the performance of the MLE-R, LSE, LSE-RTS, PF, and MPJE methods. In the LOS localization scenario with $\sigma_{d,i,k} = 0.5$, $\sigma_{v,i,k} = 0.3$, and two anchors, MPJE, LSE, and LSE-RTS are much better than MLE-R and PF methods, where the performance of LSE-RTS is higher.

B. Performance Evaluation in NLOS Environments

Unlike the LOS scenarios, there are many positions in the NLOS scenario where there is only one LOS anchor, as shown in Fig. 8. In this case, for the LSE method, the condition (32) cannot be satisfied. Therefore, the supplementing strategy for insufficient LOS measurements, that is selecting some NLOS anchors with the shorter range measurements and treating them as LOS anchors, is utilized to guarantee the condition (32).

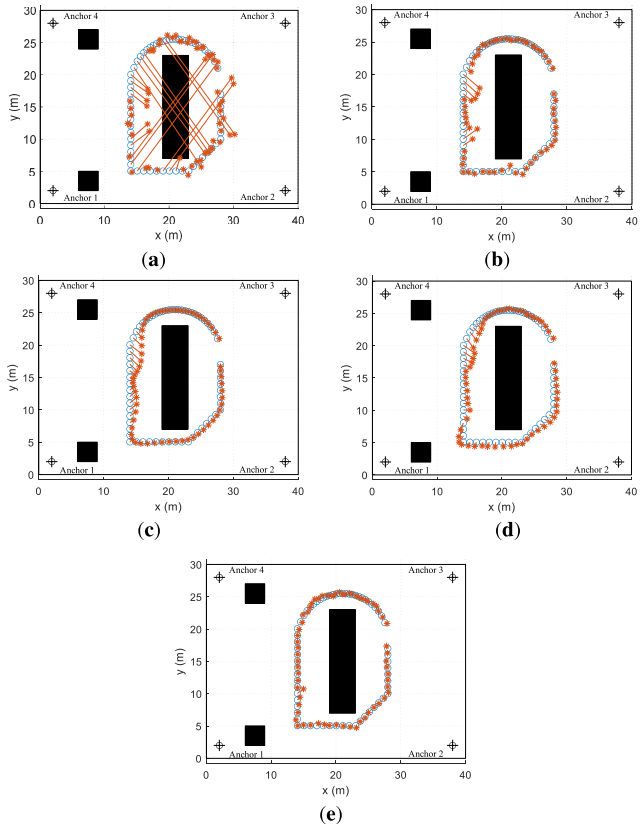

Fig. 11. NLOS localization results based on different methods. (a) MLE-R. (b) LSE. (c) LSE-RTS. (d) PF. (e) MPJE.

The standard deviation of range and relative velocity measurements are set as $\sigma_{d,i,k} = 0.3$ and $\sigma_{v,i,k} = 0.2$, respectively, where $i = 1, \ldots, 4$. For the MLE-R and LSE method, the limited searching area is defined as $x^k \in [0, 40]$ (m) and $y^k \in [0, 30]$ (m). The sequence length and LOS measurements redundancy threshold of the MPJE method is set as $T_k = 4$ and $R_{\text{thd}} = 6$, while the weight matrix is set as $\boldsymbol{w}_d^k = \boldsymbol{w}_v^k = 1$. The localization results are shown in Fig. 11.

For the MLE-R method, the introduction of the NLOS measurements severely impairs the localization precision at the positions with only one LOS anchor. Many positions fail to be localized, as shown in Fig. 11(a). This also demonstrates that the NLOS phenomenon poses a significant challenge to conventional range-based localization methods.

The impact of NLOS range measurements could be significantly mitigated by incorporating the relative velocity measurements. In Fig. 11(b)–(e), the localization performance at positions with insufficient LOS measurements is significantly improved by using LSE, LSE-RTS, PF, and MPJE method. Particularly, the MPJE method demonstrates outstanding performance in such NLOS localization scenarios.

By repeatedly performing the simulation 1000 times, the performance of these five methods is investigated, and the cdf of localization errors is drawn in Fig. 12. The confidence probabilities of localization error being less than 0.6 m for the MLE-R, LSE, LSE-RTS, PF, and MPJE methods are 60%, 80%, 76%, 66%, and 90%, respectively, where MPJE performs the best.

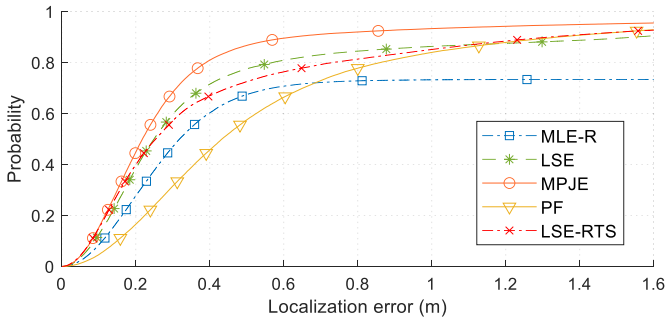

Fig. 12. CDF of the localization errors in the NLOS scenario with $\sigma_{d,i,k} = 0.3$, $\sigma_{v,i,k} = 0.2$, and four anchors.

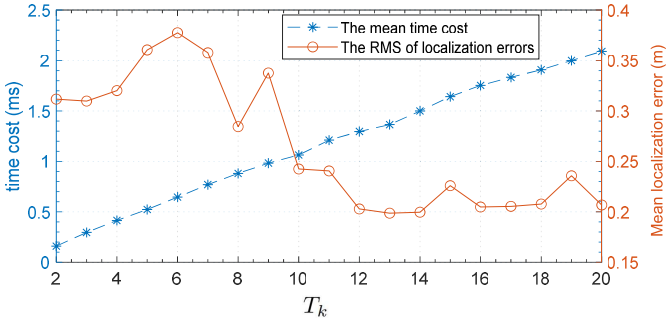

Fig. 13. Influence of T_k on the algorithm time cost and localization error.

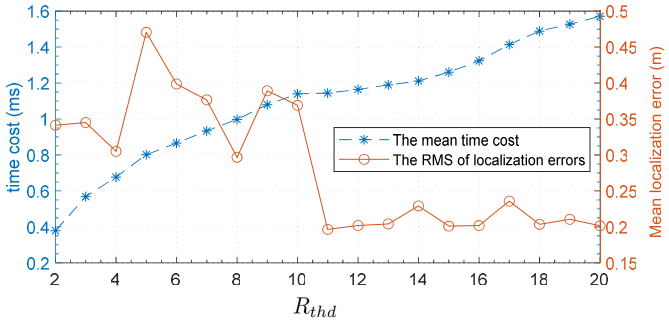

Fig. 14. Influence of R_{thd} on the algorithm time cost and localization error.

C. Choice of T_k and R_{thd}

The choice of the sequence length T_k and the LOS measurements redundancy threshold R_k directly impacts the localization performance and the computation time cost. In the given scenario, keeping the noise level of measurements and algorithm parameters constant, the values of T_k and R_{thd} are set within the interval $[2, 20]$. The experiment is repeated 1000 times to investigate how the mean localization error and algorithmic time cost vary with T_k and R_{thd}. The results are shown in Figs. 13 and 14, respectively.

The investigated results demonstrate that the localization precision improves with the increase of T_k and R_{thd}, while the algorithm time cost also increases. However, an excessively large T_k or R_{thd} will make it disadvantageous to utilize the proposed MPJE algorithm on consumer smart devices with limited computing power. Since the sequence length T_k is dynamically determined by the R_{thd}, we can set $R_{\text{thd}} \in [4, 12]$ based on the results shown in Fig. 14. The mean time cost of

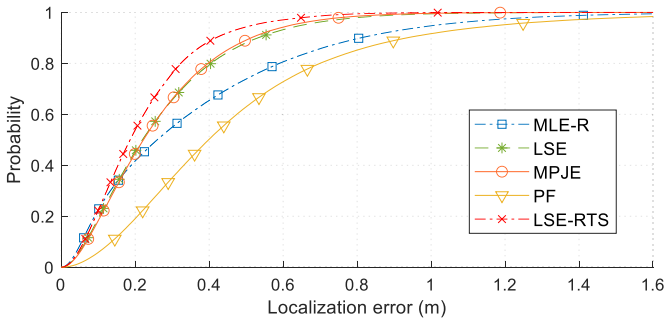

Fig. 15. CDF of the localization errors in the LOS scenario with two anchors.

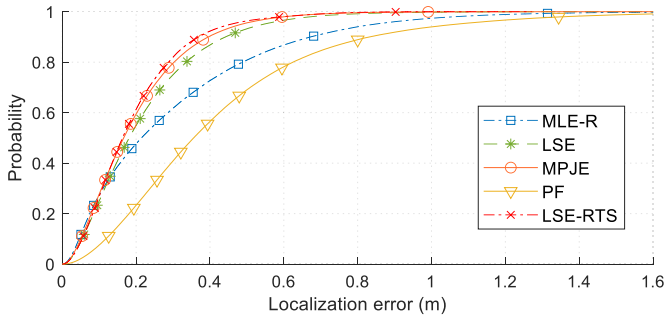

Fig. 16. CDF of the localization errors in the LOS scenario with three anchors.

MPJE at $R_{\text{thd}} = 4$ is 0.67 ms, while at $R_{\text{thd}} = 12$ is 1.16 ms. In comparison, the mean time costs of MLE-R and LSE are 3.12 and 6.15 ms, respectively, due to the high computation complexity of the numerical searching process.

D. Influence of Noise and Weight Matrix

In this section, the performance of MLE-R, LSE, LSE-RTS, PF, and MPJE is evaluated by adding different noise intensities to the measurements. The sequence length and LOS measurements redundancy threshold of the MPJE method is set as $T_k = 4$ and $R_{\text{thd}} = 6$, while the weight matrix is set as $\boldsymbol{w}_d^k = \boldsymbol{w}_v^k = 1$.

In the LOS scenario, the simulations are performed under two anchors and three anchors. Because both simulations satisfy the conditions with sufficient LOS measurements, we directly present the mean localization errors of the five localization methods with $\sigma_{d,i,k} = \{0.05, 0.1, 0.2, 0.3, 0.4, 0.5\}$ and $\sigma_{v,i,k} = \{0.05, 0.1, 0.15, 0.2, 0.25, 0.3\}$. The simulations are repeated 1000 times and the results are shown in Figs. 15 and 16.

As the increase of the density of LOS anchors, the performance of the five localization methods is all improved. The performance of the MPJE method is slightly superior to that of the LSE method. After applying RTS smoothing to the results of LSE, the LSE-RTS method demonstrates the best positioning performance in the LOS localization scenarios.

In the NLOS scenario, the overall performance of the five methods is evaluated by iterating the noise standard deviation of distance and velocity measurements in $\sigma_{d,i,k} = \{0.05, 0.1, 0.2, 0.3, 0.4, 0.5\}$ and $\sigma_{v,i,k} = \{0.05, 0.1, 0.15, 0.2, 0.25, 0.3\}$. By repeating the experiment 1000 times, the evaluation results are shown in Fig. 17. It is found that the proposed MPJE method based on range and relative velocity measurements outperforms other methods comprehensively.

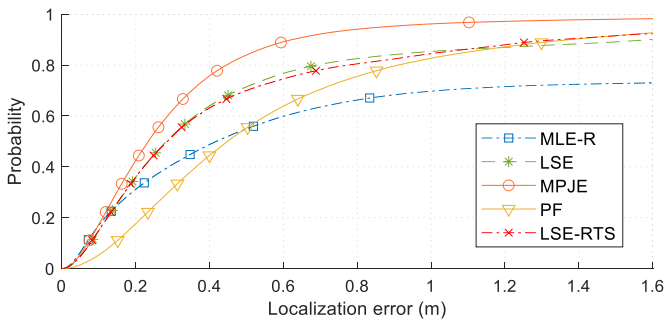

Fig. 17. CDF of the localization errors in the NLOS simulation scenario.

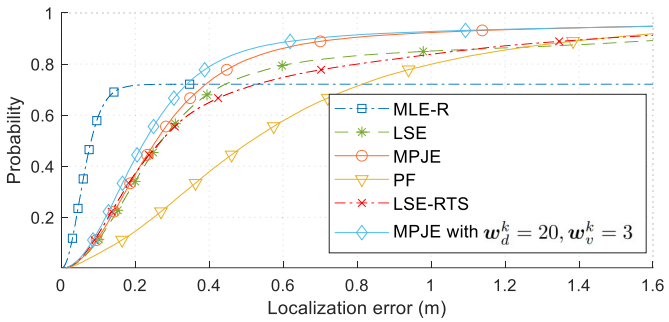

Fig. 18. CDF of the localization errors in the NLOS scenario with $\sigma_{d,i,k} = 0.05$ and $\sigma_{v,i,k} = 0.3$.

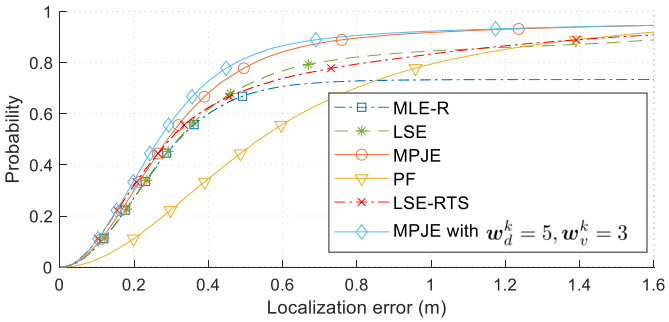

Fig. 19. CDF of the localization errors in the NLOS scenario with $\sigma_{d,i,k} = 0.2$ and $\sigma_{v,i,k} = 0.3$.

The weight matrix is another crucial factor that influences the performance of the range and relative velocity measurements-based MPJE method. As shown in Figs. 18 and 19, the performance of MPJE has been greatly improved by modifying the weight matrix based on the prior knowledge of the noise standard deviation.

The noteworthy point is that the overall performance of the MLE-R method in Fig. 18 is poor. The confidence probability of localization error being less than 0.2 m is 72%. After surpassing this critical value, the positioning error of the MLE-R method rises steeply, indicating a general lack of system stability. The introduced NLOS measurements, which are used for insufficient LOS measurement information supplement, severely limit the performance of the range-based MLE-R method.

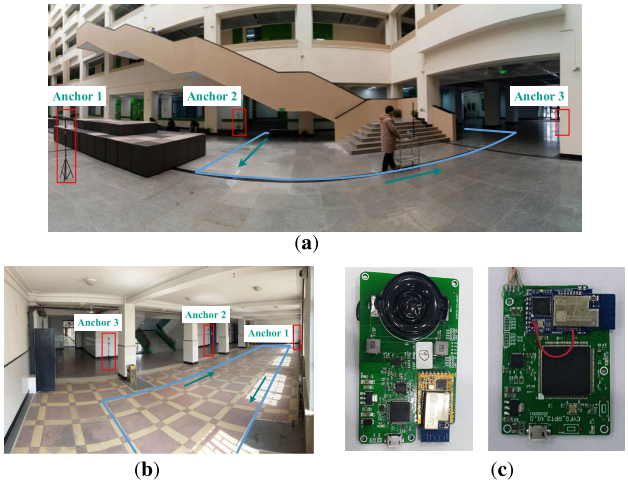

Fig. 20. Experimental scenarios. (a) Experimental scenario A. (b) Experimental scenario B. (c) Target and anchor.

As the noise pollution level of range measurements increases, the performance of range and relative velocity-based LSE and MPJE methods gradually outperforms the conventional MLE-R method. An extremely accurate range is very difficult to realize in the real world, especially in dense NLOS environments. Consequently, the range and relative velocity-based LSE and MPJE methods are more suitable for practical applications. Furthermore, the MPJE method consistently outperforms the LSE, LSE-RTS, and PF methods regardless of the level of noise pollution in measurements.

V. Experiments and Results

Experiments were conducted separately in Xiuyuan teaching building (scenario A) and the main teaching building (scenario B) at Chang'an University to test the performance of the proposed methods in a real-world setting. The size of scenario A is 24×16 (m), and the experimental space is partitioned into a lobby and corridor environment with bearing columns, walls, and stairs. The size of scenario B is 19.5×11 (m). By utilizing the four bearing columns, an NLOS localization environment can be constructed in the real world. The scenarios and devices used in this experiment are shown in Fig. 20.

The target and anchors are specially designed low-cost modules with acoustic broadcasting and sampling functions, respectively. To simplify the experiment, we use the broadcaster device as a target, and the receiver as an anchor. The audio components of the devices consist of STM32F107 and WM8978 chips, which are both inexpensive and easily accessible. The total cost of these components is less than \$5. In order to achieve one-way ranging, the local time of the target and anchor is synchronized using a LoRa module, which provides high time synchronization precision for the low propagation speed of acoustic signals.

For the measuring signal, the parameters of HFM_1 are $\{f_l, f_h, T\} = \{19.5\ \text{kHz}, 21.5\ \text{kHz}, 0.05\ \text{s}\}$. Correspondingly, the parameters of HFM_2 are $\{18.5\ \text{kHz}, 16.5\ \text{kHz}, 0.05\ \text{s}\}$. The spectrogram of the received acoustic signal is shown in Fig. 21. The background noise in scenario A is 59 dB, while

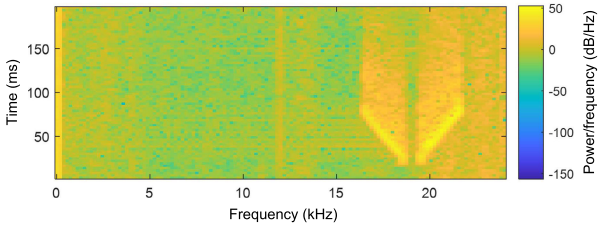

Fig. 21. Spectrogram of the measuring signal.

the background noise in scenario B is 55 dB. The target is carried by an actor who walks at a normal speed along the predefined reference paths shown in Fig. 20.

The sampling frequency of the devices is 48 kHz. The update frequency of the acoustic localization system is 1 Hz. Since the ground-truth coordinates cannot be recorded directly, we calculate the minimum distance between the estimated positions and the predefined reference path as the localization errors [4].

A. Experiments and Results in Scenario A

Experimental scenario A represents a common hybrid environment, incorporating elements from both a hall and a corridor. Upon analysis of the scenario in Fig. 22, it is evident that only one LOS anchor is located at a considerable distance below and to the left of the predefined reference path, posing a substantial challenge for all positioning algorithms. The target is affixed to a cart, operated by an actor. During the experiments, the actor pushing the cart will carefully monitor the geometric relations between his body and the anchor's position to minimize the impact of body occlusion on the experiment.

Three anchors (receivers) are securely fastened to tripods with a height of 1.6 m. The anchors' coordinates are $(21.29, 12.87)^T$ (m), $(21.16, 0.16)^T$ (m), and $(4.98, 12.8)^T$ (m), respectively. Throughout the experiments, the target is fixed on a cart, which an actor propels along a predefined reference path to ensure the smoothness of the target's motion. The predefined reference path follows a closed-loop rectangular trajectory, originating at coordinates $(19.85, 10.15)^T$ (m) and traversing points $(6.21, 10.15)^T$ (m), $(6.21, 1.1)^T$ (m), and $(19.85, 1.1)^T$ (m).

For the MLE-R and LSE method, the limited searching area is defined as $x^k \in [-3, 24]$ (m) and $y^k \in [0, 16]$ (m). The sequence length and LOS measurements redundancy threshold of the MPJE method are set as $T_k = 4$ and $R_{\text{thd}} = 6$, while the weight matrix is set as $\boldsymbol{w}_d^k = \boldsymbol{w}_v^k = 1$. Subsequently, the localization results are depicted in Fig. 22, while Fig. 23 illustrates the cdf of the localization errors.

From the localization results presented in the figures, it is evident that methods based on range and relative velocity measurements outperform the conventional range-based localization method. Specifically, for the LSE and PF methods, when the number of LOS anchors is 1, the NLOS measurements introduced by the supplemental strategy cause considerable localization errors and lead to unstable performance. By incorporating RTS smoothing, the performance

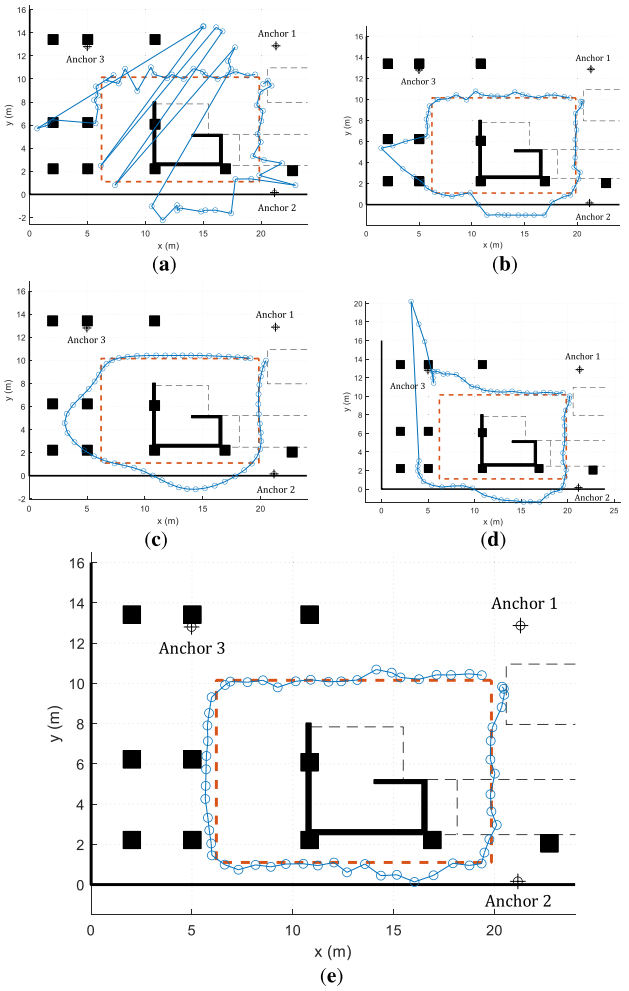

Fig. 22. Localization results in scenario A. (a) MLE-R. (b) LSE. (c) LSE-RTS. (d) PF. (e) MPJE.

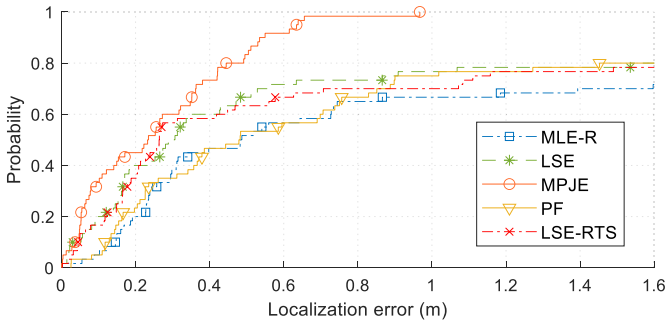

Fig. 23. CDF of the localization errors in scenario A.

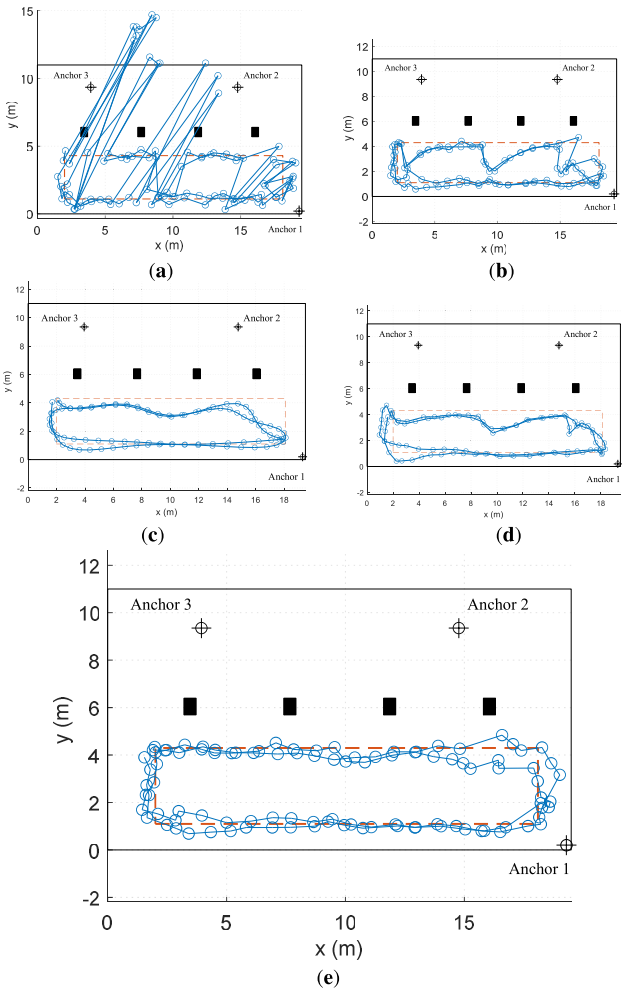

Fig. 24. Localization results in scenario B. (a) MLE-R. (b) LSE. (c) LSE-RTS. (d) PF. (e) MPJE.

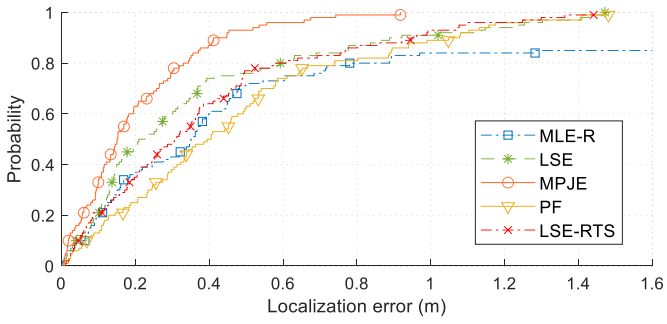

Fig. 25. CDF of the localization errors in scenario B.

of LSE shows some improvement. The MPJE method demonstrates remarkable performance in this experimental setting, showcasing superior accuracy and stability in positioning.

B. Experiments and Results in Scenario B

Following the same setup as in experimental scenario A, the height of the three anchors (receivers) is 1.6 m. They are positioned on the opposite side of the bearing columns to create the NLOS localization environment. The anchors' coordinates are $(19.3, 0.2)^T$ (m), $(14.77, 9.35)^T$ (m), and $(3.94, 9.35)^T$ (m), respectively. The actor elevates the target to reduce movement relative to the body and proceeds at a steady pace along the predefined reference path, which traces a closed-loop rectangular trajectory. The trajectory starts at coordinates $(2, 1.1)^T$ (m) and passes through points $(18.1, 1.1)^T$ (m), $(18.1, 4.3)^T$ (m), and $(2, 4.3)^T$ (m).

For the MLE-R and LSE methods, the limited searching area is defined as $x^k \in [0, 20]$ (m) and $y^k \in [0, 15]$ (m). The sequence length and LOS measurements redundancy threshold of the MPJE method are set as $T_k = 4$ and $R_{\text{thd}} = 6$, while the weight matrix is set as $\boldsymbol{w}_d^k = \boldsymbol{w}_v^k = 1$. Then, the localization

results are shown in Fig. 24. And the cdf of the localization errors illustrated in Fig. 25.

Clearly, the two experiments can produce similar conclusions, highlighting the superior positioning accuracy and stability demonstrated by the MPJE method. Comparing Figs. 23 and 25 reveals the differing positioning accuracy of systems utilizing the MPJE algorithm in various scenarios, showing influence from the localization environment and anchor deployment geometries.

VI. Conclusion

In this article, we have focused on addressing the acoustic indoor localization problem in dense NLOS environments and have proposed a range and relative velocity measurements-based localization method, without the need for additional sensors. To achieve precise localization in dense NLOS environments, an MPJE method is proposed by jointly estimating the multiple positions in a short-time position sequence, and solved by the LM algorithm.

Through the investigations by performing the numerical simulations and experiments in the real world, we can conclude that 1) using range and relative velocity measurements to realize acoustic indoor localization is an efficient way to address the localization problem in dense NLOS enviornments; 2) the proposed range and relative velocity-based LSE method could realize accurate NLOS localization and reduce the number of required LOS anchors from 3 to 2 for 2-D positioning; 3) the proposed MPJE method is an efficient NLOS localization method, and requires only two LOS anchors and permits the use of only one LOS anchor for a short period; and 4) the proposed acoustic indoor localization methods are not only suitable for dense NLOS localization scenarios but also capable of achieving accurate localization under low anchor deployment density conditions.

The main advantages of the proposed MPJE method are: 1) utilizing only LOS measurements for position estimation; in case of insufficient LOS measurements, extending the sequence length to obtain enough LOS measurement information from historical data effectively prevents the impact of NLOS measurements on the localization results; 2) requiring only two LOS anchors for precise positioning and permitting just one LOS anchor temporarily; and 3) when LOS measurements are abundant, both the precision of position estimation and the computational complexity outperform the numerical search-based LSE method. The primary limitation of this method arises when the sequence length becomes excessive, leading to a high-dimensional Jacobian matrix and Hessian matrix during the calculation in the LM algorithm, thus requiring significant memory consumption and calculation complexity. Therefore, in future work, the focus will be on optimizing the computational complexity to enable real-time application on COTS devices with limited computational capabilities.

References

[1] K. Han, B. Liu, and Z. Deng, "A tightly coupled positioning method of ranging signal and IMU based on NLOS recognition," in *Proc. IEEE 12th Int. Conf. Indoor Positioning Indoor Navigat. (IPIN)*, Sep. 2022, pp. 1–8.

[2] B. Yang, E. Yang, L. Yu, and A. Loeliger, "High-precision UWB-based localisation for UAV in extremely confined environments," *IEEE Sensors J.*, vol. 22, no. 1, pp. 1020–1029, Jan. 2022.

[3] X. Kong, C. Wu, Y. You, and Y. Yuan, "Hybrid indoor positioning method of BLE and PDR based on adaptive feedback EKF with low BLE deployment density," *IEEE Trans. Instrum. Meas.*, vol. 72, pp. 1–12, 2023.

[4] R. Chen et al., "Precise indoor positioning based on acoustic ranging in smartphone," *IEEE Trans. Instrum. Meas.*, vol. 70, pp. 1–12, 2021.

[5] H. Wang, C. Xue, Z. Wang, L. Zhang, X. Luo, and X. Wang, "Smartphone-based pedestrian NLOS positioning based on acoustics and IMU parameter estimation," *IEEE Sensors J.*, vol. 22, no. 23, pp. 23095–23108, Dec. 2022.

[6] S. Cao, X. Chen, X. Zhang, and X. Chen, "Improving the tracking accuracy of TDMA-based acoustic indoor positioning systems using a novel error correction method," *IEEE Sensors J.*, vol. 22, no. 6, pp. 5427–5436, Mar. 2022.

[7] X. Wang, C. Zhang, F. Liu, Y. Dong, and X. Xu, "Exponentially weighted particle filter for simultaneous localization and mapping based on magnetic field measurements," *IEEE Trans. Instrum. Meas.*, vol. 66, no. 7, pp. 1658–1667, Jul. 2017.

[8] L. Zhang, D. Huang, X. Wang, C. Schindelhauer, and Z. Wang, "Acoustic NLOS identification using acoustic channel characteristics for smartphone indoor localization," *Sensors*, vol. 17, no. 4, p. 727, Mar. 2017.

[9] P. S. Farahsari, A. Farahzadi, J. Rezazadeh, and A. Bagheri, "A survey on indoor positioning systems for IoT-based applications," *IEEE Internet Things J.*, vol. 9, no. 10, pp. 7680–7699, May 2022.

[10] A. Ens et al., "Acoustic self-calibrating system for indoor smartphone tracking," *Int. J. Navigat. Observ.*, vol. 2015, pp. 1–15, Feb. 2015.

[11] L. Zhang, M. Chen, X. Wang, and Z. Wang, "TOA estimation of chirp signal in dense multipath environment for low-cost acoustic ranging," *IEEE Trans. Instrum. Meas.*, vol. 68, no. 2, pp. 355–367, Feb. 2019.

[12] K. Liu, X. Liu, and X. Li, "Guoguo: Enabling fine-grained smartphone localization via acoustic anchors," *IEEE Trans. Mobile Comput.*, vol. 15, no. 5, pp. 1144–1156, May 2016.

[13] S. I. Lopes, J. M. Vieira, J. Reis, D. Albuquerque, and N. B. Carvalho, "Accurate smartphone indoor positioning using a WSN infrastructure and non-invasive audio for TDoA estimation," *Pervasive Mobile Comput.*, vol. 20, pp. 29–46, Jul. 2015.

[14] Microsoft. *Microsoft Indoor Localization and Competition IPSN 2018*. Accessed: Jan. 2, 2024. [Online]. Available: https://www.microsoft.com/en-us/research/event/microsoft-indoor-localization-competition-ipsn-2018

[15] F. Wang, H. Tang, and J. Chen, "Survey on NLOS identification and error mitigation for UWB indoor positioning," *Electronics*, vol. 12, no. 7, p. 1678, Apr. 2023.

[16] Y. Huang, Y. Zhang, Z. Wu, N. Li, and J. Chambers, "A novel robust student's t-based Kalman filter," *IEEE Trans. Aerosp. Electron. Syst.*, vol. 53, no. 1, pp. 1545–1554, Feb. 2017.

[17] Y. Huang, Y. Zhang, Y. Zhao, and J. A. Chambers, "A novel robust Gaussian-student's T mixture distribution based Kalman filter," *IEEE Trans. Signal Process.*, vol. 67, no. 13, pp. 3606–3620, Jul. 2019.

[18] Y. Huang, Y. Zhang, Y. Zhao, P. Shi, and J. A. Chambers, "A novel outlier-robust Kalman filtering framework based on statistical similarity measure," *IEEE Trans. Autom. Control*, vol. 66, no. 6, pp. 2677–2692, Jun. 2021.

[19] I. Guvenc and C.-C. Chong, "A survey on TOA based wireless localization and NLOS mitigation techniques," *IEEE Commun. Surveys Tuts.*, vol. 11, no. 3, pp. 107–124, 3rd Quart., 2009.

[20] B. Qu, L. Zhang, T. Zhang, X. Feng, X. Wang, and W. He, "OODT: LOS signal identification for acoustic indoor localization from stream perspective," *IEEE Sensors J.*, vol. 23, no. 20, pp. 24729–24743, Oct. 2023.

[21] K. Wang, Z.-H. Dong, and S.-L. Wu, "Research on FOA and TOA estimation algorithm of Galileo SAR signal," in *Proc. 2nd Int. Conf. Inf. Eng. Comput. Sci.*, Wuhan, China, Dec. 2010, pp. 1–5.

[22] V. B. Nicolau, M. Coulon, Y. Grégoire, T. Calmettes, and J. -Y. Tourneret, "Performance of TOA and FOA-based localization for Cospas-Sarsat search and rescue signals," in *Proc. 5th IEEE Int. Workshop Comput. Adv. Multi-Sensor Adapt. Process. (CAMSAP)*, St. Martin, France, 2013, pp. 312–315.

[23] L. A. Romero and J. Mason, "Geolocation using TOA, FOA, and altitude information at singular geometries," *IEEE Trans. Aerosp. Electron. Syst.*, vol. 51, no. 2, pp. 1069–1078, Apr. 2015.

[24] Y. Wang and Y. Wu, "An improved direct position determination algorithm with combined time delay and Doppler," *J. Xi'an Jiaotong Univ.*, vol. 49, no. 4, pp. 123–129, 2015.
[25] Z. Xu, C. J. Baker, and S. Pooni, "Range and Doppler cell migration in wideband automotive radar," *IEEE Trans. Veh. Technol.*, vol. 68, no. 6, pp. 5527–5536, Jun. 2019.
[26] T. Jia, K. C. Ho, H. Wang, and X. Shen, "Effect of sensor motion on time delay and Doppler shift localization: Analysis and solution," *IEEE Trans. Signal Process.*, vol. 67, no. 22, pp. 5881–5895, Nov. 2019.
[27] T. Jia, K. C. Ho, H. Wang, and X. Shen, "Localization of a moving object with sensors in motion by time delays and Doppler shifts," *IEEE Trans. Signal Process.*, vol. 68, pp. 5824–5841, 2020.
[28] A. J. Weiss, "Direct geolocation of wideband emitters based on delay and Doppler," *IEEE Trans. Signal Process.*, vol. 59, no. 6, pp. 2513–2521, Jun. 2011.
[29] X. Chen, D. Wang, R.-R. Liu, J.-X. Yin, and Y. Wu, "Structural total least squares algorithm for locating multiple disjoint sources based on AOA/TOA/FOA in the presence of system error," *Frontiers Inf. Technol. Electron. Eng.*, vol. 19, no. 7, pp. 917–936, Sep. 2018.
[30] R.-R. Liu, Y.-L. Wang, J.-X. Yin, D. Wang, and Y. Wu, "Passive source localization using importance sampling based on TOA and FOA measurements," *Frontiers Inf. Technol. Electron. Eng.*, vol. 18, no. 8, pp. 1167–1179, Aug. 2017.
[31] C. Jia, J. Yin, Z. Yang, and L. Zhang, "Position and velocity estimation using TOA and FOA based on Lagrange programming neural network," *J. Phys., Conf. Ser.*, vol. 1284, no. 1, Aug. 2019, Art. no. 012064.
[32] J. Shi, G. Wang, and L. Jin, "Moving source localization using TOA and FOA measurements with imperfect synchronization," *Signal Process.*, vol. 186, Sep. 2021, Art. no. 108113.
[33] R. Ramlall, J. Chen, and A. L. Swindlehurst, "Non-line-of-sight mobile station positioning algorithm using TOA, AOA, and Doppler-shift," in *Proc. Ubiquitous Positioning Indoor Navigat. Location Based Service (UPINLBS)*, 2014, pp. 180–184.
[34] L. Zhang, W. Liu, J. Zhou, and X. Bai, "TOA and FOA based acoustic indoor localization in NLOS environment," in *Proc. IEEE Int. Conf. Signal Process., Commun. Comput. (ICSPCC)*, Zhengzhou, China, Nov. 2023.
[35] Z. Gu and S. Fang, "Joint range-Doppler estimation based on multipulse processing of composite hyperbolic frequency modulated waveforms," *IEEE Signal Process. Lett.*, vol. 29, pp. 558–562, 2022.
[36] H. Kuttruff, *Room Acoustic*, 4th ed. London, U.K.: Spon Press, 2006, pp. 89–114.
[37] H. P. Gavin, "The Levenberg–Marquardt algorithm for nonlinear least squares curve-fitting problems," Dept. Civil Environ. Eng., Duke Univ., Durham, NC, USA, Tech. Rep., 2019, vol. 19. [Online]. Available: https://people.duke.edu/~hpgavin/ExperimentalSystems/lm.pdf
[38] K. Madsen, H. B. Nielsen, and O. Tingleff. *Methods for Non-linear Least Squares Problems*. Accessed: Jan. 2, 2024. [Online]. Available: http://www2.imm.dtu.dk/pubdb/edoc/imm3215.pdf
[39] M. Sun, Y. Gao, Z. Jiao, Y. Xu, Y. Zhuang, and P. Qian, "R-T-S assisted Kalman filtering for robot localization using UWB measurement," in *Proc. Mobile Netw. Appl.*, Apr. 2022, pp. 1–10.

Lei Zhang received the B.Eng. and M.Sc. degrees in mechanical engineering from Chang'an University, Xi'an, China, in 2007 and 2013, respectively, and the Ph.D. degree in control science and engineering from Zhejiang University, Hangzhou, China, in 2019.

Presently, he serves as a Lecturer with the School of Construction Machinery, Chang'an University. His research interests encompass machine learning, acoustic signal processing, time–frequency analysis, indoor positioning, and tracking.

Hucheng Wang (Member, IEEE) received the B.Eng. degree in information and communication technology in 2015, and the joint Ph.D. degree in cyberspace security from the Guilin University of Electronic Technology, Guilin, China, and Zhejiang University, Hangzhou, China, in 2023.

He is currently a Postdoctoral Researcher with the School of Computer Science and Technology, Yangtze Delta Region Academy, Beijing Institute of Technology, Jiaxing, China. His research interests include indoor localization, acoustic signal processing, data fusion, NLoS recognition, and federal learning.

Dr. Wang is a Young Professional.

Wei He received the B.E. degree in biomedical engineering from Tianjin University, Tianjin, China, in 2002, the M.E. degree in biomedical engineering from the University of Science and Technology of China, Hefei, China, in 2005, and the Ph.D. degree in communication and information system from the University of Chinese Academy of Sciences, Beijing, China, in 2013.

He is now a Research Fellow with the Shanghai Institute of Microsystem and Information Technology, Chinese Academy of Sciences, Beijing. His research interests include wireless sensor networks, deep learning, target detection, and localization.

Xinheng Wang (Senior Member, IEEE) received the B.E. and M.Sc. degrees in electrical engineering from Xi'an Jiaotong University, Xi'an, China, in 1991 and 1994, respectively, and the Ph.D. degree in electrical engineering from Brunel University, Uxbridge, U.K., in 2001.

He is currently a Professor with the School of Advanced Technology and was the Founding Head of the Department of Mechatronics and Robotics, Xi'an Jiaotong-Liverpool University (XJTLU), Suzhou, China. Prior to joining XJTLU, he was a professor with different universities in the U.K. He has been an Investigator or Co-Investigator of nearly 30 research projects sponsored by EU, U.K. EPSRC, Innovate U.K., China NSFC, and industry. He has authored or coauthored more than 220 refereed articles. He holds 15 granted patents, including one U.S., Japanese, four South Korean, and nine Chinese patents. He was one of the key developers of the world's first smart trolley to provide intelligent services to passengers at airports. His current research interests include intelligent and connected systems, including robotics and healthcare, and indoor localization and navigation for robots and human beings. He is also interested in the digitalization of traditional Chinese medicine and posture detection by acoustic analysis on smartphones.